Cobalt nanoparticles trigger ferroptosis-like cell death (oxytosis) in neuronal cells : Potential implications for neurodegenerative disease

Gupta, Govind

2020-04

Gupta , G , Gliga , A , Hedberg , J , Serra , A , Greco , D , Odnevall Wallinder , I & Fadeel , B 2020 , ' Cobalt nanoparticles trigger ferroptosis-like cell death (oxytosis) in neuronal cells : Potential implications for neurodegenerative disease ' , FASEB Journal , vol. 34 , no. 4 , pp. 5262-5281 . https://doi.org/10.1096/fj.201902191RR

http://hdl.handle.net/10138/317347
https://doi.org/10.1096/fj.201902191RR

Received: 27 August 2019 | Revised: 23 January 2020 | Accepted: 1 February 2020

DOI: 10.1096/fj.201902191RR

RESEARCH ARTICLE

THE FASEB JOURNAL

Cobalt nanoparticles trigger ferroptosis-like cell death (oxytosis) in neuronal cells: Potential implications for neurodegenerative disease

Govind Gupta[1] | **Anda Gliga**[2] | **Jonas Hedberg**[3] | **Angela Serra**[4,5] | **Dario Greco**[4,5] | **Inger Odnevall Wallinder**[3] | **Bengt Fadeel**[1]

[1]Unit of Molecular Toxicology, Institute of Environmental Medicine, Karolinska Institutet, Stockholm, Sweden

[2]Unit of Metals and Health, Institute of Environmental Medicine, Karolinska Institutet, Stockholm, Sweden

[3]Division of Surface and Corrosion Science, Department of Chemistry, Royal Institute of Technology, Stockholm, Sweden

[4]Institute of Biosciences and Medical Technologies, University of Tampere, Tampere, Finland

[5]Institute of Biotechnology, University of Helsinki, Helsinki, Finland

Correspondence
Bengt Fadeel, Unit of Molecular Toxicology, Institute of Environmental Medicine, Karolinska Institutet, Nobels väg 13, Karolinska Institutet, 171 77 Stockholm, Sweden.
Email: bengt.fadeel@ki.se

Funding information
Swedish Foundation for Strategic Environmental Research

Abstract

The neurotoxicity of hard metal-based nanoparticles (NPs) remains poorly understood. Here, we deployed the human neuroblastoma cell line SH-SY5Y differentiated or not into dopaminergic- and cholinergic-like neurons to study the impact of tungsten carbide (WC) NPs, WC NPs sintered with cobalt (Co), or Co NPs *versus* soluble $CoCl_2$. Co NPs and Co salt triggered a dose-dependent cytotoxicity with an increase in cytosolic calcium, lipid peroxidation, and depletion of glutathione (GSH). Co NPs and Co salt also suppressed glutathione peroxidase 4 (GPX4) mRNA and protein expression. Co-exposed cells were rescued by N-acetylcysteine (NAC), a precursor of GSH, and partially by liproxstatin-1, an inhibitor of lipid peroxidation. Furthermore, in silico analyses predicted a significant correlation, based on similarities in gene expression profiles, between Co-containing NPs and Parkinson's disease, and changes in the expression of selected genes were validated by RT-PCR. Finally, experiments using primary human dopaminergic neurons demonstrated cytotoxicity and GSH depletion in response to Co NPs and $CoCl_2$ with loss of axonal integrity. Overall, these data point to a marked neurotoxic potential of Co-based but not WC NPs and show that neuronal cell death may occur through a ferroptosis-like mechanism.

KEYWORDS

cobalt, ferroptosis, hard metal, nanoparticles, neurodegeneration, oxytosis

1 | INTRODUCTION

Hard metal is an alloy based on tungsten carbide (WC) and cobalt (Co). Occupational exposure during the production of hard metal is associated with several adverse health effects with the respiratory tract being one of the main targets.[1] Prolonged exposure to Co has also been shown to be associated with cardiomyopathy.[2] Furthermore, Co is classified as possibly carcinogenic

Abbreviations: DLS, dynamic light scattering; FBS, fetal bovine serum; GPX4, glutathione peroxidase 4; GSH, glutathione; IARC, International Agency for Research on Cancer; ICP-MS, inductively coupled plasma mass spectrometry; iPSC, induced pluripotent stem cell; LAL, Limulus amebocyte lysate; L-dopa, levodopa; MPTP, 1-methyl-4-phenyl-1,2,3,6-tetrahydropyridine; NAC, N-acetylcysteine; NPs, nanoparticles; PCCS, photon cross-correlation spectroscopy; PD, Parkinson's disease; RA, retinoic acid; ROS, reactive oxygen species; SLC7A11, solute carrier family 7 member 11; TH, tyrosine hydroxylase.

to humans (group 2B) by the International Agency for Research on Cancer (IARC). In recent years, the use and production of hard metal has increased considerably. One such example is tire studs, with pins made of WC sintered with Co, used in many countries during the winter to improve gripping power on icy roads. However, their use is controversial as hard metal nanoparticles (NPs) are released into the environment due to the wear of such studs, which could lead to adverse health effects.[3]

Co has also been widely used in biomedical applications including in hip prostheses and this, in turn, may give rise to internal exposure to Co resulting in significant systemic concentrations of Co.[4] Indeed, health concerns have been raised due to the release of potentially toxic levels of Co (and chromium, Cr) by hip implants used in orthopedic surgery.[5,6] In a recent study, Scharf et al[7] performed histological and elemental analyses in Cr and Co exposed patients undergoing hip revision surgery and were able to document a positive correlation between the amounts of Cr^{3+} and Co^{2+} ions in tissues and oxidative damage. Furthermore, anecdotal evidence has been put forward for a link between the corrosion of metal-bearing hip prostheses and neurological symptoms.[8] In another case report, the authors found a correlation between Parkinson's disease (PD) symptoms and prosthesis wear-induced hypercobaltemia.[9] However, despite these case reports, there are few systematic studies on the neurotoxicity of Co or hard metal-based NPs. Bastian et al[10] examined acute cytotoxicity of WC and WC-Co (10 wt% Co) NPs in various human cell lines as well as in rat neuronal and glial cells and found that WC-Co NPs significantly decreased viability in oligodendrocytes and astrocytes when compared with WC NPs. More recently, Zheng et al[11] have shown that Co NPs and $CoCl_2$ caused neurotoxicity in rats as well as in PC-12 cells (derived from a rat pheochromocytoma) with NPs showing greater toxic potency when compared to $CoCl_2$. Notwithstanding, the studies performed to date fall short in terms of providing a detailed understanding of the mechanism of neurotoxicity of Co-based particles and the potential relation of these materials with neurodegenerative diseases in humans. Therefore, we investigated the potential impact of WC, WC-Co (5 wt% Co), and Co NPs in a human neuroblastoma cell line in comparison to $CoCl_2$ and elucidated the underlying mechanism of cell death in these cells. Furthermore, we explored the relation of Co-based NPs with PD by using an in silico approach[12] coupled with in vitro validation in our cell model, and we verified our findings in primary human dopaminergic neurons cultivated ex vivo. Overall, our results provide new insights regarding the neurotoxicity of Co.

2 | MATERIALS AND METHODS

2.1 | Particle characterization

WC, WC-Co, and Co NPs were purchased from American Elements (Los Angeles, CA). WC-Co NPs (product code WC-CO-03 MNP. 200N; <200 nm, 40-80 nm) contained 5 wt% Co and had a purity of 99.9%. According to the manufacturer, Co was precipitated on WC NPs *via* wet chemistry to produce WC-Co NPs. Co NPs (product code CO-M-028M-NP.100N, <100 nm) had a purity of 99.8%. WC NPs (product code W-C-03M-NP.100N, <100 nm) had a purity of 99.9%. Water soluble Co (II) chloride ($CoCl_2{\cdot}6H_2O$; Sigma) was included as ionic control at equivalent concentrations of the Co NPs. NP dispersions were made freshly at stock concentration of 1 mg/mL in endotoxin-free water followed by 4 minutes sonication for WC and Co NPs and 7 minutes for WC-Co NPs at 10% amplitude using a probe sonicator (Branson Sonifier S-450D, Branson Ultrasonics Corp., Danbury, CT). Subsequent dilutions were immediately prepared in cell medium prior to exposure. Endotoxin content was evaluated by using the chromogenic Limulus amebocyte lysate (LAL) assay (Lonza, Walkersville, MD), as described.[13] The samples were endotoxin-free (data not shown). The primary size of the NPs was determined by transmission electron microscopy (TEM)[14] and representative images are shown. Hydrodynamic size distribution and zeta potential of NP suspensions (50 μg/mL) in water and two different cell culture media (see below) was measured at 1 and 24 hours by dynamic light scattering (DLS) using a Malvern Zetasizer Nano ZS instrument equipped with 4.0 mW, 633 nm laser (Model ZEN3600, Malvern Instruments Ltd., UK) as described.[13] NP stability and sedimentation in cell media was determined by photon cross-correlation spectroscopy (PCCS).[15] In brief, PCCS (NanoPhox, Sympatec) was used to analyze NP dispersions (50 μg/mL) immediately after dispersion (5 minutes), and after 1 and 24 hours. Triplicate samples were analyzed to obtain the size distribution patterns. Calibration was performed using standard latex samples (20 ± 2 nm).

2.2 | Human neuronal cell line

The human neuroblastoma cell line (SH-SY5Y) was obtained from Sigma-Aldrich (cat no. 94030304) and cultured in DMEM/F12:MEME (1:1) cell medium (Sigma-Aldrich) supplemented with heat-inactivated fetal bovine serum (FBS) (10%), glutamine (2 mM), penicillin and streptomycin, and nonessential amino acids (Sigma-Aldrich). The cell cultures were regularly tested for mycoplasma contamination. SH-SY5Y cells were also differentiated into dopaminergic/cholinergic-like neurons using retinoic acid (RA) (1 μM) (Sigma-Aldrich) in DMEM/F12 medium supplemented with glutamine (2 mM), penicillin and streptomycin, and N2 growth factor supplement (ThermoFisher). SH-SY5Y cells were differentiated up to 6 days and cell medium of differentiating cells was replenished after 3 days to ensure availability of optimal nutrients and differentiation factor for the growth of cells. Differentiation of cells was checked on the last day by expression analysis of selected genes used as markers for

dopaminergic (monoamine oxidase A *[MAOA]* and neurogenin 2 [*NeuroG2]*) and cholinergic neurons (choline acetyltransferase *[CHAT]* and solute carrier family 18 member A3 [*SLC18A3]*) by using RT-PCR (see below). Cytotoxicity of NPs was evaluated before and after differentiation of SH-SY5Y cells into cholinergic/dopaminergic neurons. To this end, SH-SY5Y cells were seeded at a density of 2.5×10^4 cells/cm^2 for undifferentiated cells and 1.25×10^4 cells/cm^2 for differentiating or differentiated cells. After 24 hours, particle dispersions were directly added to the cell cultures to achieve a final concentration of 0, 1, 5, 10, 20, 50, and 100 μg/mL. The final volume used in 6- or 96-well plates was 2.7 and 0.1 mL, respectively, in order to maintain the same μg/cm^2 concentration between experiments. The exposure in undifferentiated and differentiated cells was maintained for 24 hours; however, in differentiating cells, NPs were added at day 1 and cell medium was replenished after 3 days without adding NPs and the cells were then maintained up to day 6. To probe the mechanism of cell death induced by Co, cells were co-exposed with Co (20 and 50 μg/mL) and inhibitors of apoptosis (zVAD-fmk, 20 μM), necroptosis (necrostatin-1, 30 μM), ferroptosis (liproxstatin-1, 10 μM), autophagy (wortmannin, 1 μM), as well as deferoxamine (10 μM). These inhibitors were all purchased from Sigma-Aldrich (Sweden). The cells were preincubated with the indicated inhibitors for 30 minutes prior to exposure to NPs or $CoCl_2$. Loss of cell viability was determined by using the Alamar blue assay (ThermoFisher Scientific).[13] Data are derived from three independent experiments each performed in triplicate.

2.3 | Primary human neurons

Predifferentiated dopaminergic neurons (or DOPA precursors) (ASE-9323) derived from a karyotype normal human induced pluripotent stem cell (iPSC) line were purchased from Applied StemCell (Milpitas, CA). The cells were cultured and differentiated to produce primary dopaminergic neurons (mature DOPA neurons) by applying the optimized dopaminergic maturation medium and supplements provided by Applied StemCell (ASE-9323DM). Briefly, before seeding the cells the culture vessels were coated with 20 μg/mL of poly-L-ornithine (Sigma-Aldrich) and vessels were incubated for 2 hours at 37°C (5% CO_2). Next, the vessels were rinsed with ultrapure water and 10 μg/mL of laminin solution (ThermoFisher) was added to cover the bottom of each vessel followed by another incubation for 2 hours at 37°C (5% CO_2). Afterward, laminin was aspirated and DOPA precursors cells (4.0×10^4 cells/cm^2) were seeded evenly in the vessels without further washing and cells were placed in the cell culture incubator. During the entire process of dopaminergic neuron maturation, two types of complete medium were used as provided by the supplier: Medium A (DOPA Medium + Supplement A) was used for culture from day 0-4; whereas Medium B (DOPA Medium + Supplement B) was used for culture from day 4-12. The cell medium was changed every other day up to 12 days. At 12 days, the cells were immunostained with anti-TH and Tuj-1 antibodies (see below) to confirm the differentiation status. NPs and Co salt exposure to the cells was performed at day 4 and day 12 in the cell media indicated above and exposures were maintained for 24 hours. After exposure, cell viability and glutathione (GSH) content was determined by using Alamar blue and GSH-Glow^{TM} assays, respectively. Control and treatment groups were also imaged under an optical microscope to capture morphological changes.

2.4 | Inductively coupled plasma mass spectrometry (ICP-MS)

SH-SY5Y cells were seeded at 0.5×10^6 cells per well 1 day before the experiment and then exposed for 24 hours to freshly dispersed NPs at a final concentration of 10 μg/mL. After exposure, the cells were collected by trypsinization followed by washing three times with PBS and then processed for metal analysis by ICP-MS. For Co release in cell medium and water, NPs were freshly dispersed at 10 μg/mL and incubated for 0 and 24, at 37°C. After incubation, the particle dispersions were centrifuged at 15,000 rpm, 1 hour (0°C) and the supernatants were carefully collected. Non-centrifuged dispersions were also collected in order to measure the total amount of W or Co added. The samples were digested in 32% of HNO_3 for at least 48 hours to ensure complete mineralization. Before analysis, all the samples were diluted to reach approximately 2% of HNO_3. For all samples, Co and W isotopes were quantified using an iCAP Q ICP-MS (Thermo Scientific) instrument in KED mode. Calibration standards of 0.1, 1, 10, and 100 μg/L Co and W were prepared using a 1000 mg/L reference standard (Spectrascan). Samples spiked with 12.25 μg/L of indium were used as an internal standard with a range of recovery between 80% and 100%. Each sample was injected at least three times and the RSD acceptance was set at 15%. Cell uptake results were normalized according to the cell number and expressed as pg Co/cell. Co release was expressed as the percentage Co released in cell medium or water in relation to the amount of total Co added.

2.5 | Transmission electron microscopy

To visualize cellular uptake of NPs and to assess any ultrastructural changes, cells were incubated with 10 μg/mL of WC, WC-Co, and Co NPs for 24 hours. Samples were then

processed for TEM.[16] Briefly, samples were washed three times with serum-free medium and fixed with 4% of glutaldehyde in 0.1 M of sodium phosphate buffer pH 7.4 for 1 hour at 4°C. Following postfixation in 1% of OsO_4 in 0.1 sodium phosphate buffer for 1 hour at 4°C, the samples were serially dehydrated in gradient of ethanol followed by acetone and LX-112 infiltration and finally embedded in LX-112. Ultrathin sections (approximately 50-80 nm) were prepared using a Leica EM UC6, contrasted with uranyl acetate followed by lead citrate, and examined in Hitachi HT 7700 electron microscope (Hitachi). Images were acquired using a 2k × 2k Veleta CCD camera (Olympus).

2.6 | Flow cytometry

For the analysis of mitochondrial membrane potential, cells were seeded in 6-well plates and exposed to Co NPs and $CoCl_2$ at the indicated concentrations for 1 and 6 hours. After exposure, SH-SY5Y cells were incubated for 30 minutes at 37°C in the dark with the cell permeable, fluorescent probe, tetramethylrhodamine, ethyl ester (TMRE) (25 nM). Cells were then trypsinized, neutralized with cell culture medium, and the cell pellet was resuspended in HEPES buffer (10 mM HEPES-NaOH, 150 mM NaCl, 5 mM KCl, 1 mM $MgCl_2$, and 1.8 mM $CaCl_2$, pH 7.4). Fluorescence was recorded using a BD LSRFortessa flow cytometer operating with BD FACS DIVA software (BD Biosciences). Cellular debris was gated out and ten thousand events were collected for each sample. Data were analyzed using FCS express software (BD Biosciences). For determination of intracellular calcium levels, cells exposed with the indicated concentrations of NPs for 1 hour and then incubated with 5 μM of Fluo-4-acetoxymethyl ester (Fluo-4 AM, ThermoFischer Scientific, in 3% of DMSO) for 30 minutes at 37°C. Fluorescence was recorded using a BD LSRFortessa flow cytometer operating with BD FACS DIVA™ software (BD Biosciences). In order to investigate whether chelation in intracellular and/or extracellular Ca^{2+} can modulate the toxicity of Co NPs and salt, SH-SY5Y cells were co-exposed to Co NP (20 and 50 μg/mL) and EDTA (1 mM, Sigma), EGTA (1 mM, Sigma), and BAPTA-AM (5 μM, ThermoScientific) for 24 hours, and cytotoxicity was evaluated using Alamar blue assay. Cells were preincubated with chelators for 30 minutes prior to Co exposure.

2.7 | Confocal microscopy

SH-SY5Y cells were grown on coverslips in 24-well plates and then exposed to the Co NPs and $CoCl_2$ at 20 μg/mL for 12 hours. After exposure, the cells were washed thrice and incubated with 0.5 μM of MitoTracker Red (Invitrogen) for 30 minutes. The cells were then fixed in 3% of paraformaldehyde in phosphate buffer at room temperature for 20 minutes followed by washing with PBS. The coverslips were mounted on glass slides with VECTASHIELD Antifade Mounting Medium with DAPI (Invitrogen) and a Zeiss LSM880 confocal microscope equipped with a laser diode 405 nm, argon laser 488 nm, and HeNe1 543 nm was used to analyze the samples. Additionally, SH-SY5Y cells were grown on coverslips in 24-well plates and exposed to the mitochondrial uncoupling agent, CCCP (carbonyl cyanide m-chlorophenyl hydrazine) (Sigma-Aldrich) (50 μM) or Co NPs and $CoCl_2$ at 50 μg/mL for 6 hours. SH-SY5Y cells were then washed and incubated for 30 minutes at 37°C in the dark with the cell permeable, fluorescent dye, tetramethylrhodamine, ethyl ester (TMRE) (25 nM) that is sequestered by active mitochondria. To monitor lipid peroxidation, SH-SY5Y cells were loaded with 2.5 μM of the oxidation-sensitive probe $C11\text{-}BODIPY_{581/591}$ for 30 minutes. After washing with PBS, cells were fixed in 4% of paraformaldehyde and washed again and mounted on glass slides using VECTASHIELD Antifade Mounting Medium with DAPI. Confocal imaging was performed as described above.

2.8 | Immunocytochemistry

The differentiation of DOPA precursor cells to mature DOPA neurons was confirmed by immunostaining of 12-day differentiated cells for tyrosine hydroxylase (TH) and anti-β3-tubulin (Tuj-1) expression. To this end, cells were seeded at a density of 4.0×10^4 cells/cm^2 and grown on glass coverslips in 24-well plates. At day 12, cells were washed and fixed in 4% of formaldehyde for 15 minutes at room temperature. Then, coverslips were washed in PBS and permeabilized in 0.1% of Triton-X 100 (Sigma-Aldrich) for 15 minutes, followed by blocking with 10% of goat serum (Abcam) and 0.1% of Triton-X100 for 60 minutes. Then, coverslips were incubated with mouse anti-Tuj-1 antibody (Sigma-Aldrich) or rabbit anti-TH antibody (Abcam) in antibody buffer (8% of goat serum and 0.1% of Triton-X-100) overnight at 4°C. Coverslips were then rinsed in PBS and incubated with secondary antibodies, goat anti-mouse antibody 680 Alexa conjugated (Abcam) and goat anti-rabbit antibody 480 Alexa conjugated (Abcam), for 1 hour. Coverslips were mounted on glass slides using DAPI-containing mounting medium (Invitrogen) and imaged using a Zeiss LSM880 microscope.

2.9 | Spectrophotometric assays

For reactive oxygen species (ROS) production, cells were seeded in a 96-well plate 1 day before the experiment to allow

cells to adhere. The following day, cells were loaded with 10 μM of H_2-DCF (Invitrogen) and incubated for 30 minutes in the dark, at 37°C and 5% CO_2. The cells were washed at least twice after completion of incubation and supplemented with fresh cell medium. DCF-loaded cells were exposed at the indicated concentrations of Co NPs and salt for 1 hour. DCF fluorescence (ex/em—485/535 nm) was recorded using the Tecan Infinite® 200 plate reader (Männedorf, Switzerland). In order to investigate whether increased ROS is involved in the toxicity of Co NPs and salt, SH-SY5Y cells were co-exposed to Co NP (20 and 50 μg/mL) and ascorbic acid (100 μM) or mitoTEMPO (100 μM) (both from Sigma-Aldrich) for 12 hours, and cytotoxicity was evaluated using Alamar blue assay, as described above. For GSH levels, SH-SY5Y cells (1.0×10^4 cells/well) were seeded in 96-well plate and exposed with 5, 10, and 20 μg/mL of WC, WC-Co, Co NPs, and Co for 6 hours. After exposure, cell medium was discarded and samples were analyzed by using the GSH-Glow™ assay (Promega). Briefly, GSH-Glow™ reagent was added to wells and incubated for 30 minutes at room temperature followed by adding luciferin detection reagent. The luminescence was measured using a Tecan Infinite® 200 plate reader. In order to investigate whether alterations in intracellular GSH can modulate the toxicity of Co NPs and salt, SH-SY5Y cells were co-exposed to Co NP or Co ions (20 and 50 μg/mL) and N-acetylcysteine (NAC) (2.5 mM) (Sigma-Aldrich) or GSH (0.5 mM) (Sigma-Aldrich) for 12 hours, and cytotoxicity was evaluated using Alamar blue assay (see above). Cells were preincubated with NAC and GSH for 30 minutes before the administration of Co NPs or $CoCl_2$.

To complement the results obtained using Fluo-4 AM, SH-SY5Y cells (6.0×10^4 cells/well) were seeded in 96-well plates and exposed to 20 and 50 μg/mL of WC, WC-Co, Co NPs, and Co salt for 1 hour. Cells were exposed in DMEM/F12:MEM or calcium-free DMEM/F12:S-MEM (ThermoFischer Scientific), as indicated. Then, the cell medium was discarded and samples were analyzed by using the Fura-2 no-wash calcium assay kit (Abcam, Germany) according to the manufacturer's instructions. Briefly, the ratiometric Fura 2 dye diluted in loading buffer (Pluronic F127 plus in HHBS buffer) was added to each well and samples were incubated for 60 minutes at 37°C (5% CO_2) followed by incubation for 20 minutes at room temperature. The fluorescence was detected at Ex/Em 340/510 and Ex/Em 380/510 by using the SpectraMax MiniMax 300 imaging cytometer (Molecular Devices) (courtesy of Dr G. Sotiriou). The ratio of Ex 340/380 plotted to indicate changes in Ca^{2+} levels. For quantification of lipid peroxidation, SH-SY5Y cells were exposed to Co NPs and $CoCl_2$ at the indicated concentrations for 6 hours in the presence and absence of liproxstatin-1 (10 μM). After exposure, cells were loaded with 2.5 μM of the oxidation-sensitive probe C11-$BODIPY_{581/591}$ (Thermo Fisher Scientific) for 30 minutes and then washed with PBS. Fluorescence was measured at 484/510 nm (green) and 581/610 nm (red) using the SpectraMax® MiniMax 300 imaging cytometer. The percent increase in relative fluorescence was calculated with respect to untreated controls.

2.10 | RT-PCR

Cells were seeded in 6-well plates and exposed to RA as described above (for differentiation marker studies) or NPs at the indicated concentrations for 24 hours (undifferentiated SH-SY5Y cells) or 6 days (differentiated SH-SY5Y cells). After exposure, cells were washed with PBS and subjected to RNA isolation. RNA isolation was performed using the QIAGEN RNeasy Mini Kit according to the manufacturer's protocol. The quality and yield of RNA was checked using NanoDrop (ThermoScientific). cDNA was synthesized using iScript™ Reverse Transcriptase Kit (Bio-Rad) using a thermal cycler (Bio-Rad). RT-PCR was performed using SYBR-Green based 96-well primePCR custom plates (Bio-Rad) for the following genes: *MAOA*, *NeuroG2*, *CHAT*, *SLC18A3*, glutathione peroxidase 4 (*GPX4)*, solute carrier family 7 member 11 (*SLC7A11*), *RAF1*, *NEFH*, *RPLP1*, and *GAPDH* (Table S1). Each RT-PCR reaction contained 1 μL of cDNA, 1x SsoAdvanced universal SYBR supermix (Bio-Rad) and 1x PrimePCR assay dried in well. Reactions were performed in three technical replicates. RT-PCR was run using the AB7500 RT-PCR (Applied Biosystems) at the following conditions: activation at 95°C for 2 minutes, 40 cycles of denaturation at 95°C for 5 s, and annealing/elongation at 60°C for 30 s. The fold change in the gene expression was obtained by calculating ΔΔCt value with respect to GAPDH or RPLP1 as reference control.

2.11 | Western blot

Cell lysates were prepared by incubating cells in RIPA buffer [Tris-HCl (pH 7.4), NaCl (150 mM), NP40 (1%), Na-deoxycholate (0.25%), EDTA (1mM), dithiothreitol (1 mM), phenylmethylsulfonyl fluoride (1mM)] with a protease inhibitor cocktail (1x) added freshly just before the use for 3 hours, as described.[17] Cell lysates were centrifuged at 13000xg for 20 minutes and supernatants were collected for western blot. The protein concentration was measured by Bradford assay. Thirty μg of protein was loaded for each sample and proteins were separated by running an SDS-PAGE (4%-12% Bis-Tris gel). Proteins were transferred to PVDF membranes and incubated overnight with primary antibody at 1:1000. The rabbit polyclonal primary antibody against GPX4 was purchased from Abcam (Sweden) and a mouse anti-GAPDH antibody (Ambicon)

was used as a loading control. Membranes were washed and incubated with a goat anti-rabbit secondary antibody (1:15 000) for 1 hour. Fluorescently labeled anti-mouse or anti-rabbit secondary Ab were procured from LI-COR Biosciences (Lincoln, NE). Blots were scanned and imaged using the LI-COR Biosciences system following the manufacturer's instructions. The results were quantified by dividing the signal of the tested protein in relation to the loading control.

2.12 | In silico transcriptomics

To explore potential associations between NPs and human diseases, we employed insideNANO ("Integrated Network of Systems Biology Effects of Nanomaterials"), a web-based tool (publicly available at http://inano.biobyte.de) that highlights connections between phenotypic entities based on their effects on gene expression.[12] The tool comprises gene expression data corresponding to four different entities (ie, NPs, drugs, chemical substances, and human diseases), derived from scientific databases as described in.[12] Gene expression data for NPs were retrieved from NanoMiner, a transcriptomics database encompassing in vitro transcriptomics profiles.[18] RT-PCR-based validation (above) focused on those genes displaying the same directionality for Co-containing NPs and 1-methyl-4-phenyl-1,2,3,6-tetrahydropyridine (MPTP), a chemical known to cause PD-like symptoms. To this end, SH-SY5Y cells differentiated with RA for 6 days were utilized.

2.13 | Statistics

The results shown are derived from experiments performed at least three times. Data are presented as mean values ± SD GraphPad Prism 5 (GraphPad Inc) was used for statistical analysis. One-way ANOVA followed by Dunnett's or Tukey's *post hoc* analysis was used for the analysis of statistical significance, and $P < .05$ was considered significant.

3 | RESULTS

3.1 | Nanoparticle characterization and Co release

To understand the behavior of the NPs in relevant cell media, hydrodynamic size, zeta potential, particle stability (changes in size distribution with time), and particle dissolution/Co release were evaluated for the NPs. Figure S1 shows the results for WC, WC-Co, and Co NPs in deionized water and cell culture media (note that different cell media are used for undifferentiated and differentiated cells, see below). TEM revealed that WC and Co-based NPs were heterogeneously distributed below the 100 nm size range (Figure S1A-C). WC and WC-Co NPs were found to be more agglomerated than Co NPs. The hydrodynamic sizes of WC and Co-based NPs in water and in differentiated cell medium were in the range of 400 to 900 nm (Figure S1D-F). The average size of WC and WC-Co NPs agglomerates was reduced in the serum-containing undifferentiated cell medium. We noted a higher average size of the NPs at 1 hour due to the presence of agglomerates. However, at 24 hour, these larger sized agglomerates had sedimented from the dispersion yielding a lower average size of the remaining agglomerates in solution. Sedimentation of the NPs was further corroborated by reduced count rates in solution with time at 5 minutes, 1, and 24 hours by PCCS (Figure S1J-L). The results showed that the count rates in dispersion were drastically reduced at 24 hours indicative of sedimentation of the NPs. The zeta potentials of the NPs were in the range of −8 to −35 mV (WC > WC-Co > Co NPs) (Figure S1G-I). The zeta potential of the WC and WC-Co NPs was reduced in cell culture media with serum. Table S2 shows the release of Co from NPs. Following incubation of WC-Co and Co NP in water and the undifferentiated cell medium at 37°C (10 μg Co/mL), 11% and 35% (in water), and 80% and 15% (in cell medium), respectively, of total added Co was detected in solution immediately after dispersion at 0 hour. This is an effect of rapid dissolution mechanisms and the fact that dissolution takes place already during the sonication of stock solutions At 24 hours, 61% and 73% (in water), and 77% and 96% (in cell medium), respectively, of total added Co was detected in solution (Table S2), in line with previous work showing near-complete release of Co in synthetic surface water.[14]

3.2 | Neurotoxicity of Co-containing NPs

SH-SY5Y cells were differentiated by using RA (1 μM) up to 6 days as shown previously.[19] At day 6, these cells exhibited extended neurites typically seen in mature neurons (Figure 1A-F) and expressed specific markers of dopaminergic as well as cholinergic neurons, as determined by RT-PCR (Figure 1H). The undifferentiated, differentiating, and differentiated SH-SY5Y cells were exposed to WC, WC-Co, and Co NPs *versus* $CoCl_2$. The undifferentiated and differentiated cells were exposed for 24 hours and dose-dependent toxicity was observed for Co NPs and $CoCl_2$ in both cell models (Figure 1G,I). WC-Co NPs showed significant toxicity toward differentiated cells only at the highest dose (100 μg/mL). However, WC NPs were nontoxic to the cells. In addition, to study cells undergoing differentiation, NPs or Co salt were added at day 1 and cell

medium was replenished after 3 days without adding NPs and cells were then maintained up to day 6 (Figure S2A). To allow for a better comparison with the undifferentiated cells, cytotoxicity was also determined in undifferentiated cells at 72 hours after continuous exposure to NPs *versus* $CoCl_2$, or in undifferentiated cells exposed for 72 hours

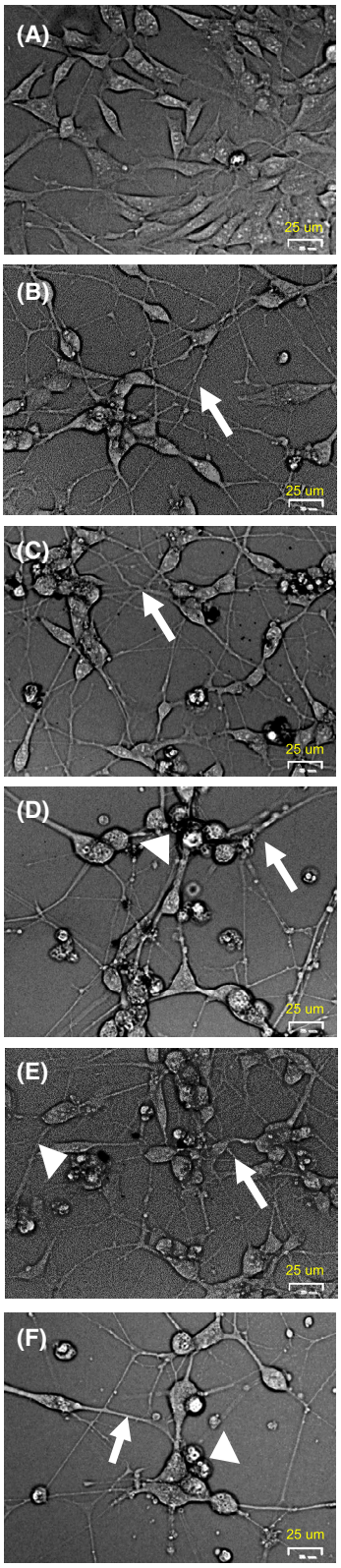

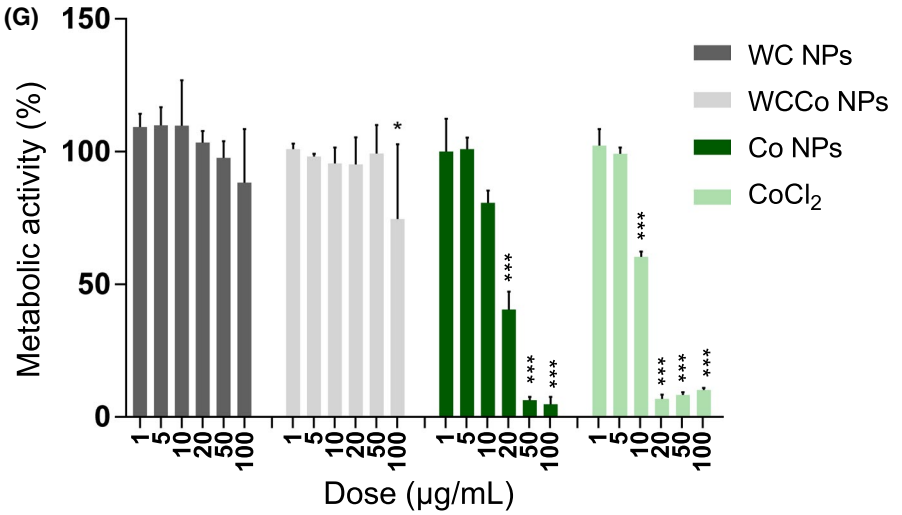

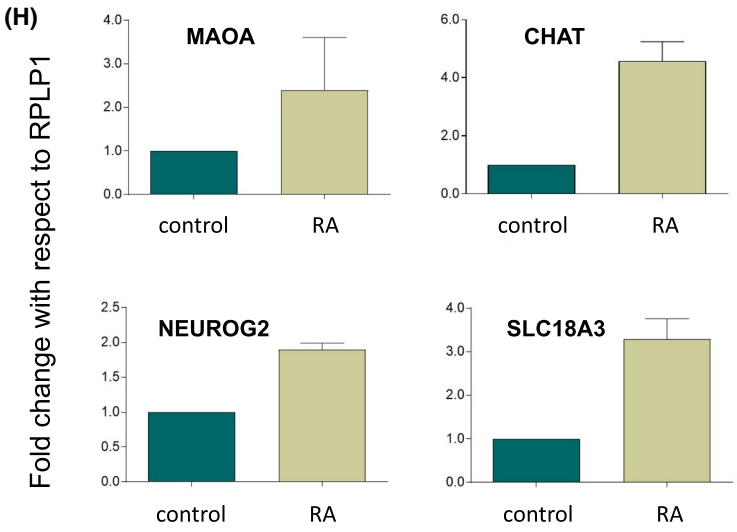

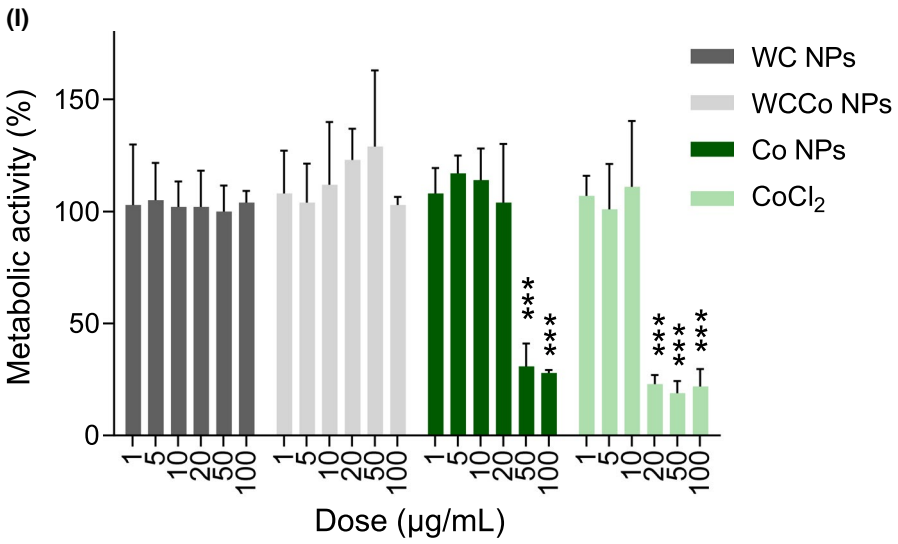

FIGURE 1 Co-induced neurotoxicity. Cytotoxicity of WC NPs, WC-Co NPs, Co NPs, and $CoCl_2$ in undifferentiated SH-SY5Y cells *versus* SH-SY5Y cells differentiated for 6 days with retinoic acid (RA) prior to exposure. Optical micrographs of cells at day 6: A, control without RA, B, control with RA, C, WC NPs, D, WC-Co NPs, E, Co NPs, F, $CoCl_2$. Arrows represent neurites that appeared after differentiation with RA. Arrowheads indicate dead cells. Metabolic activity, determined by using the Alamar blue assay, of undifferentiated cells after 24 hours (G), and differentiated cells after 24 hours (I). Data shown are mean values ± SD (n = 3). $^*P < .05$, $^{**}P < .01$, $^{***}P < .001$. H, Expression of dopaminergic and cholinergic markers after 6 days of RA (1 μM) induced differentiation. RT-PCR based analysis of the dopaminergic markers, MAOA (monoamine oxidase A) and NeuroG2 (neurogenin 2), and the cholinergic markers, CHAT (choline acetyltransferase) and SLC18A3 (solute carrier family 18 member A3). Data shown are mean values ± SD (n = 2)

and then maintained for another 72 hours in fresh medium without NPs (Figure S2B,C). This extended exposure to Co caused a similar degree of toxicity as in the differentiating cells. Overall, with regard to Co NPs and $CoCl_2$, our findings suggest that undifferentiated cells are more susceptible than cells differentiated into neuronal-like cells.

3.3 | Uptake of NPs in neuronal cells

TEM and ICP-MS was performed to understand cellular uptake and ultrastructural changes in SH-SY5Y cells following NP exposure. TEM micrographs clearly showed that WC, WC-Co, and Co NPs were internalized by the cells; furthermore, Co NPs were visualized in endosome-like vesicles (Figure 2A-L). It is interesting to note that intact Co NPs were present in the cells at 24 hours even though these NPs were found to undergo dissolution in cell culture medium (Figure 2J). Some mitochondria appeared swollen and degenerated following exposure to Co NPs (Figure 2K). In addition, fibrillary structures were noted in the cytoplasm of Co NP-exposed cells; such cytoplasmic changes are common in neurodegenerative disorders.[20] We did not observe any morphological changes of the nucleus. Furthermore, cellular content of tungsten and Co was assessed by ICP-MS 24 hours after exposure to WC, WC-Co, and Co NPs (Figure 2M-N). The cellular content of Co reached 5 pg Co/cell after Co NP exposure, which was about four times higher than the amount of Co in cells exposed to the equivalent amount of $CoCl_2$ (approximately 1 pg Co/cell), suggesting that the NPs bring more Co into cells (the so-called Trojan horse effect).

3.4 | Role of ROS and calcium homeostasis

Next, cellular ROS levels were studied in order to explore the potential role in Co toxicity. A dose-dependent increase in cellular ROS levels, as determined by using the cell permeable probe H_2-DCF, was observed following exposure of non-differentiated cells to Co NPs for 1 hour, while the impact of $CoCl_2$ was considerably less pronounced (Figure 3A-B). Co NPs and $CoCl_2$ did not elicit any drop in the mitochondrial membrane potential at 1 hour (data not shown). After 6 hours of exposure, a modest effect was noted for the Co NPs whereas $CoCl_2$ triggered a marked dissipation of the mitochondrial membrane potential (Figure 3C). Confocal imaging was performed to verify the results; CCCP was included as a positive control (Figure 3D-G). To evaluate whether ROS play a role in the cytotoxicity of Co NPs and $CoCl_2$, cells were preincubated with ascorbic acid and mitoTEMPO (a specific scavenger of mitochondrial superoxide) and cytotoxicity was determined after 24 hours. However, these experiments revealed no rescue of cell death (data not shown). Next, we determined cellular calcium levels in cells using Fluo-4 AM and found that calcium levels were increased in cells exposed to Co NPs and $CoCl_2$ (Figure 4A). To support these results, we applied the ratiometric dye, Fura 2, and incubated cells in regular cell culture medium (Figure 4B) *versus* calcium-free cell culture medium (Figure 4C). Co NPs and $CoCl_2$ were both found to trigger an increase in cytosolic calcium (at 20 μg/mL). This was noted also in the case of calcium-free medium (at a higher dose of 50 μg/mL). Modest or no effects were seen for WC and WC-Co NPs. Furthermore, calcium chelation by using different intra- and extracellular chelators prevented cell death after 24 hours of exposure to $CoCl_2$ and, to a lesser degree, Co NPs (Figure 5A-F). It is noted that EGTA and EDTA have been shown to also chelate Co ions[21] and this could potentially explain the marked effect in the case of $CoCl_2$ (at 20 μg/mL, but not at 50 μg/mL) (Figure 5B,D). BAPTA-AM, on the contrary, is a calcium-specific chelator that acts as an intracellular calcium sponge, and was shown here to protect against Co NPs and $CoCl_2$ (Figure 5E,F), though the response was less pronounced when compared to EDTA and EGTA.

3.5 | Depletion of GSH in Co-exposed cells

Non-apoptotic neuronal cell death is associated with GSH depletion.[22] To further explore the cellular responses to Co, we determined GSH levels by using the luminescent-based GSH-Glow assay in which the reaction is catalyzed by GSH S-transferase. Co NP and $CoCl_2$ exposed cells displayed a significant and dose-dependent decrease in GSH content (Figure 6A-B) while no significant change was observed in WC and WC-Co NPs exposed cells (data not shown). The Co

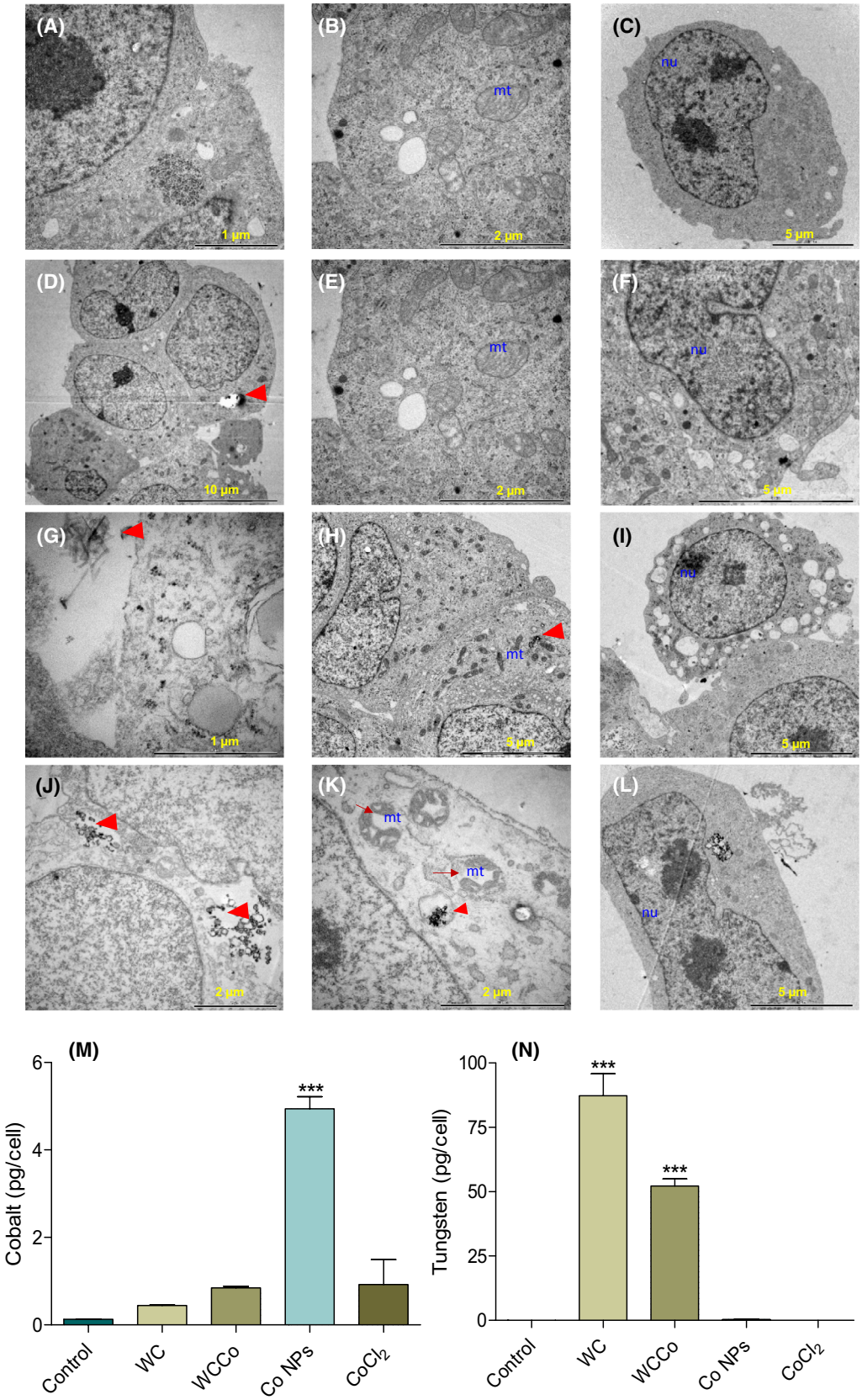

FIGURE 2 Cellular uptake of tungsten and Co-containing NPs in undifferentiated SH-SY5Y cells. A-L, TEM micrographs show cellular uptake and ultrastructural changes in SH-SY5Y cells after 24 hours of exposure with NPs at 10 µg/mL; A-C, control, D-F, WC NPs, G-I, WC-Co NPs, and J-L, Co NPs. mt—mitochondria, nu—cell nuclei. Red arrows point to abnormal mitochondria; arrowheads indicate the NPs. Scale bars are shown in each image. M-N, Cellular concentration of Co and W in cells exposed to NPs or $CoCl_2$ at 24 hours, as determined by ICP-MS. Data shown are mean values ± SD (n = 3). $^{*}P < .05$, $^{**}P < .01$, $^{***}P < .001$

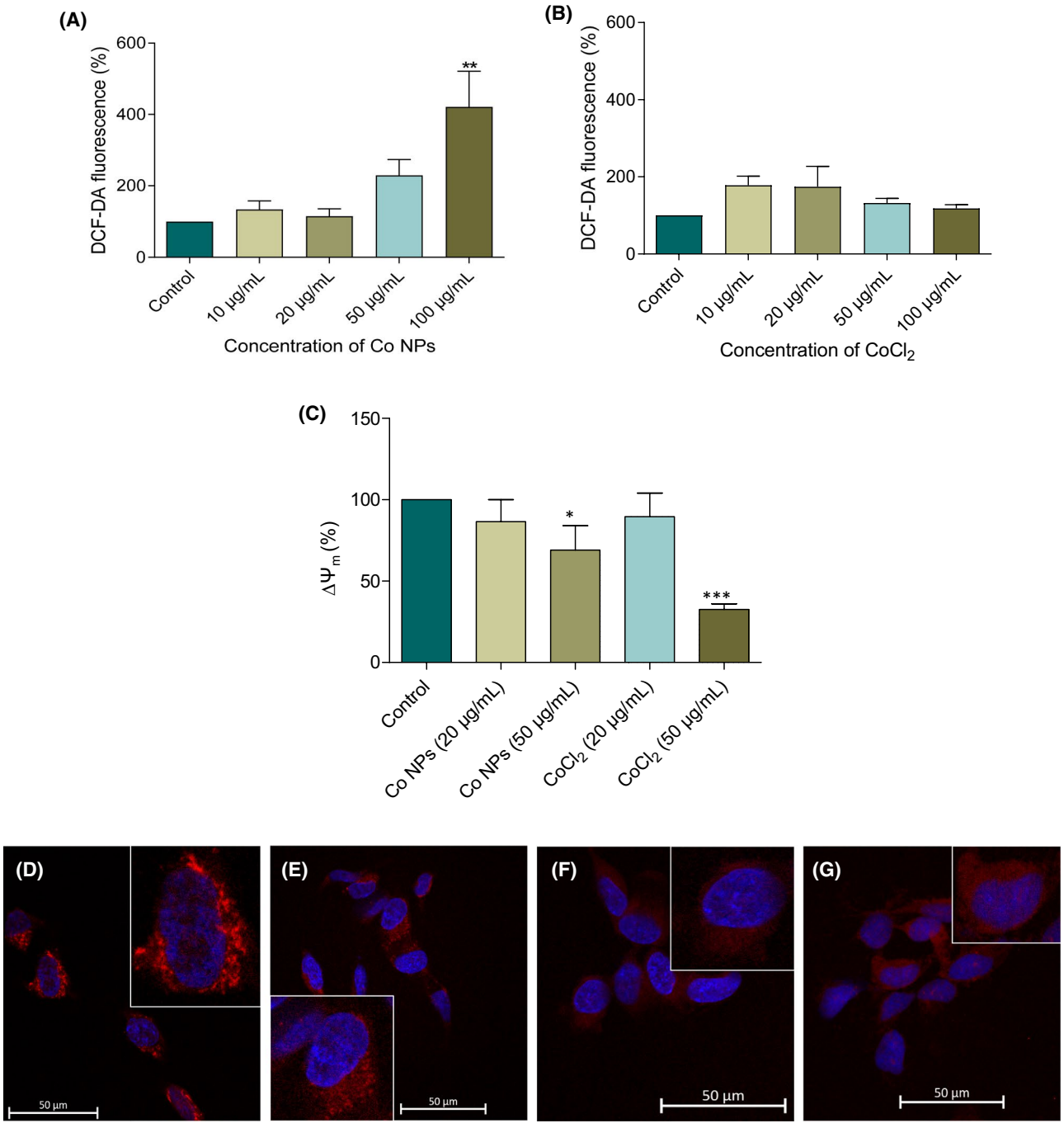

FIGURE 3 Reactive oxygen species (ROS) and mitochondrial membrane potential ($\Delta\Psi_m$) in undifferentiated SH-SY5Y cells after exposure to Co NPs and $CoCl_2$. A-B, Intracellular oxidized DCF fluorescence measured after 1 hour of exposure to the indicated concentrations of Co NPs and $CoCl_2$, respectively. C, TMRE staining shows loss of $\Delta\Psi_m$ after exposure to Co NPs and $CoCl_2$ for 6 hours (20 and 50 µg/mL). Confocal microscopy of cells stained with TMRE (red) after 6 hours: control (D), CCCP (50 µM) (E), Co NPs (50 µg/mL) (F), and $CoCl_2$ (50 µg/mL) (G). Blue fluorescence corresponds to nuclear staining with DAPI

salt showed the strongest effect as GSH dropped to almost undetectable levels within 6 hours after exposure at 10 µg/mL. Co-exposure with NAC (a GSH precursor) significantly reversed the cell death triggered by Co NPs (Figure 6C). Furthermore, NAC and GSH afforded partial protection of cells against $CoCl_2$ at 12 hours (Figure S3A,B) and 24 hours (Figure S3E,F).

3.6 | Co triggers ferroptosis-like cell death

To further enhance our understanding of the Co-mediated cell death mechanism, the impact of inhibitors of apoptosis, necroptosis, ferroptosis, and autophagy were tested. No rescue was seen following co-exposure of cells to Co NPs or $CoCl_2$ with zVAD-fmk (caspase inhibitor), necrostatin-1

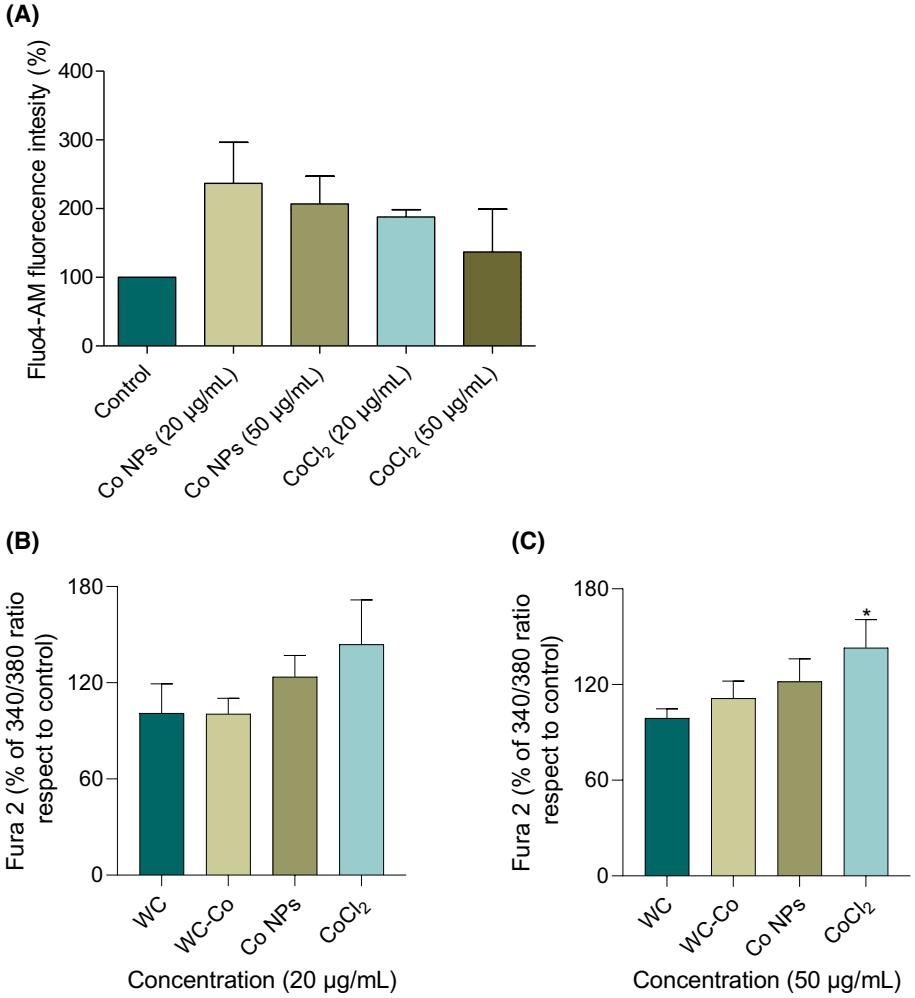

FIGURE 4 Cytosolic calcium elevation in undifferentiated SH-SY5Y cells after exposure to Co NPs and $CoCl_2$. A, Increase in intracellular calcium levels measured by using the calcium-specific fluorescent probe, Fluo-4-AM, after 1 hour of exposure. Increase in intracellular calcium levels at 1 hour was verified by using the ratiometric dye, Fura 2, for cells maintained in regular cell culture medium (20 µg/mL) (B) *versus* cells maintained in calcium-free medium (50 µg/mL) (C). Data are mean values ± SD $*P < .05$. Statistical significance values were determined by applying Tukey's *post hoc* multiple comparison test

(RIP1/3 kinase inhibitor), or wortmannin (PI3K inhibitor) (data not shown). However, liproxstatin-1, a lipid antioxidant that is known to suppress ferroptosis, partially prevented Co NP-triggered cell death (Figure 7F) and reduced $CoCl_2$-triggered cell death (Figure S3C,G). Furthermore, co-exposure with the iron chelator, deferoxamine, partially reduced cell death triggered by Co NPs (Figure 7F) as well as cell death in cells exposed to the Co salt (Figure S3D,H). Co NPs and $CoCl_2$ also triggered lipid peroxidation, as determined by spectrophotometric analysis of SH-SY5Y cells stained with C11-BODIPY$_{581/591}$ (Figure 7A,B). Furthermore, the dose-dependent increase in lipid peroxidation after Co NP and $CoCl_2$ exposure was counteracted upon co-incubation with liproxstatin-1. These results were further confirmed by confocal microscopy of exposed cells (Figure 7C-E). Lipid peroxidation-dependent cell death is believed to be regulated by GPX4, and neuron-specific GPX4 depletion causes neurodegeneration.[23] We, therefore, asked whether Co exposure had any effect on GPX4 expression. Indeed, as shown in Figure 6D, *GPX4* was decreased in SH-SY5Y cells exposed to Co NPs and $CoCl_2$. We also noted a significant decrease in GPX4 protein expression in cells exposed to Co NPs and $CoCl_2$ (20 µg/mL), but not when cells were exposed to WC or WC-Co NPs (Figure 6F, and Figure S4). We then asked whether the alterations in GSH content were related to the cystine/glutamate antiporter, system Xc^-. As shown in Figure 6E, the system Xc^- subunit *SLC7A11* was upregulated in cells after exposure to Co NPs and $CoCl_2$ (20 µg/mL), but not WC or WC-Co NPs.

3.7 | Potential link between Co and PD

Using the computational tool, insideNANO, we recently highlighted a potential association of several metal and

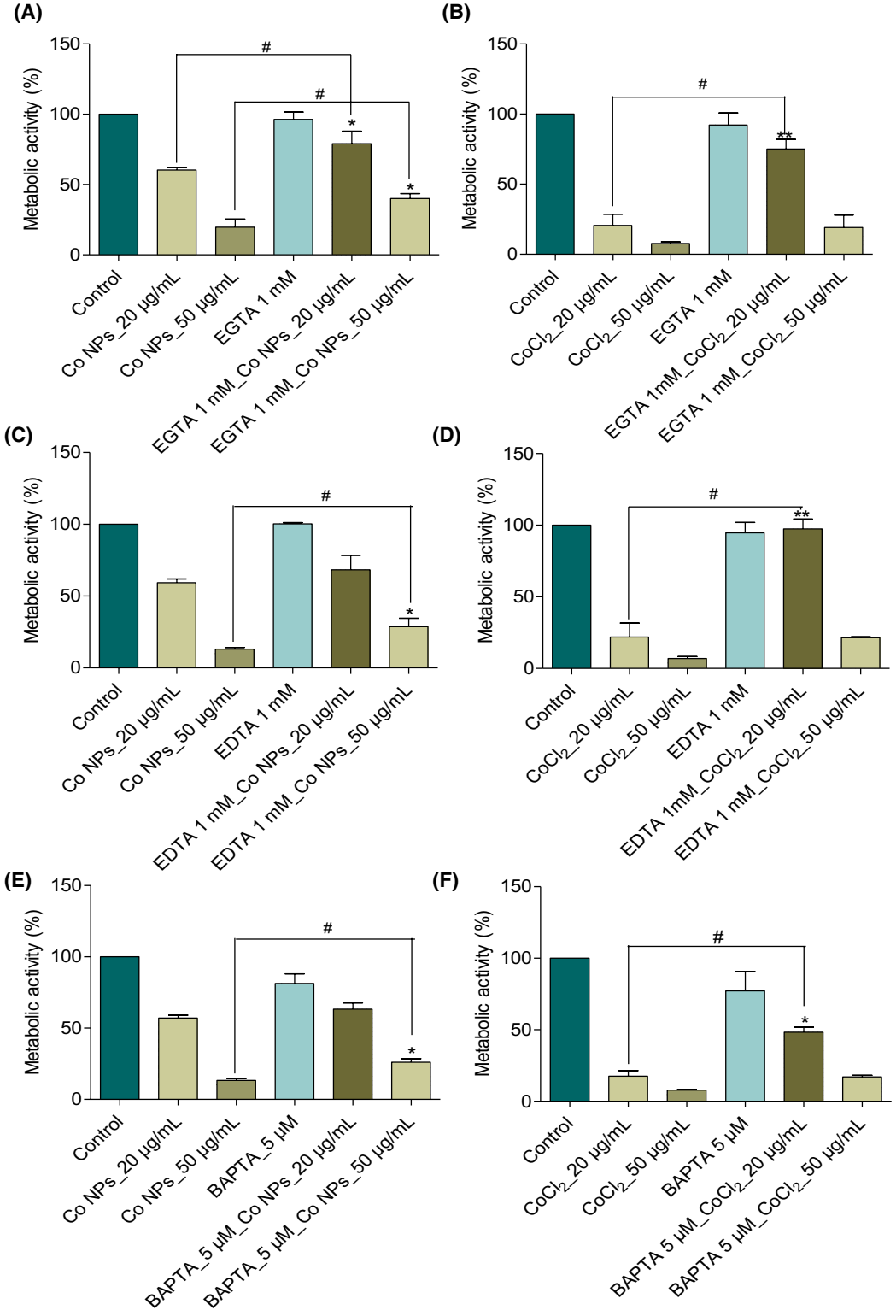

FIGURE 5 Calcium-dependent cell death in Co-exposed SH-SY5Y cells. Metabolic activity of undifferentiated cells after exposure to Co NPs or $CoCl_2$ (20 or 50 µg/mL) for 24 hours in the presence or absence of calcium chelators: A-B, EGTA (1 mM), C-D, EDTA (1 mM), and E-F, BAPTA-AM (5 µM). Data are mean values ± SD (n = 3). $^*P < .05$, $^{**}P < .01$. Statistical significance determined by applying Tukey's *post hoc* multiple comparison test

metal oxide NPs and neurodegenerative disorders, including PD.[12] One of the intriguing observations was the association, based on commonalities between transcriptional signatures, between WC and Co NPs, on the one hand, with MPTP and levodopa (L-dopa) on the other hand.[12] The corresponding results are depicted in Figure S5A. WC-Co

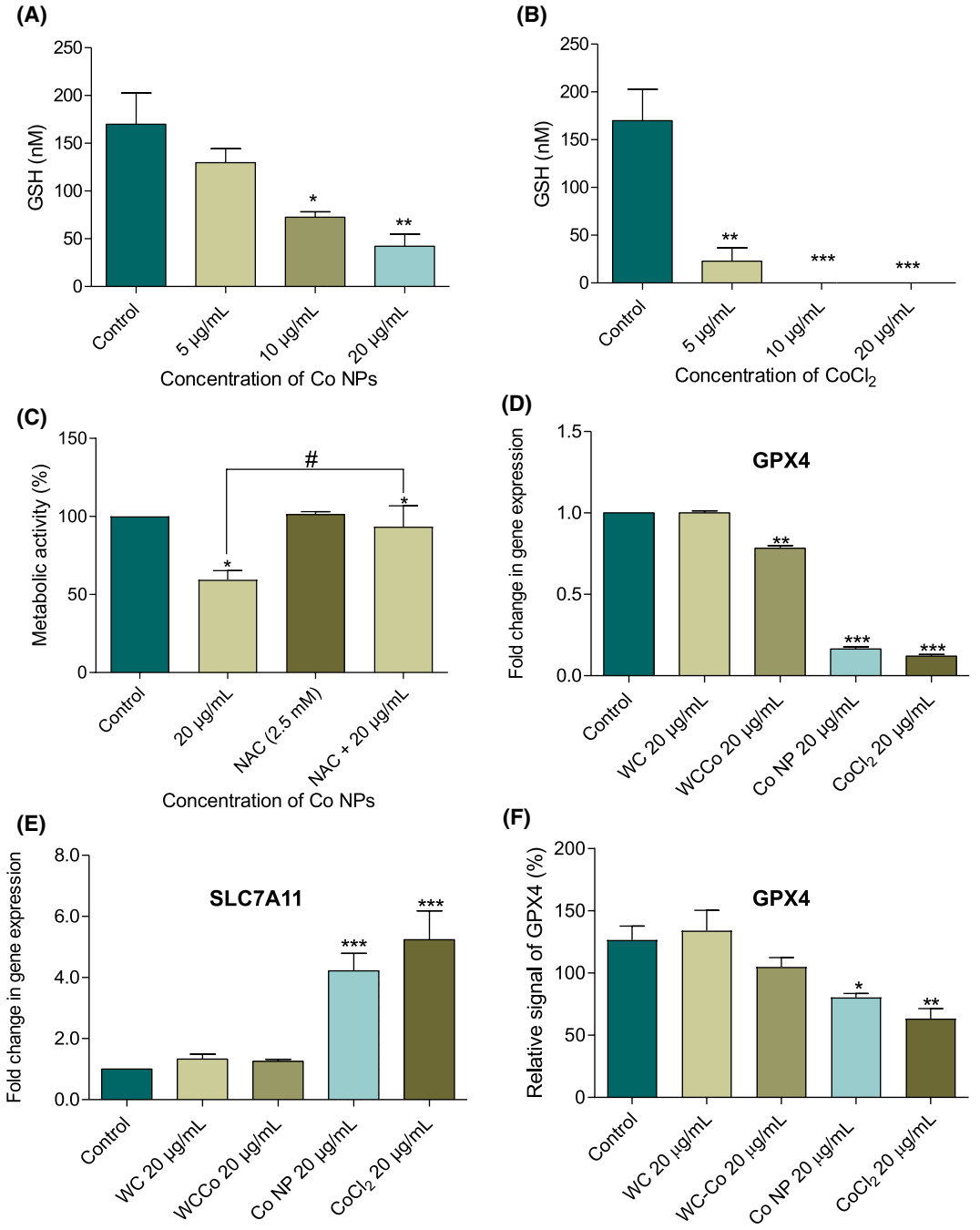

FIGURE 6 Co depletes the antioxidant, glutathione (GSH), leading to death of undifferentiated SH-SY5Y cells. GSH level in the cells after 6 hours of exposure with Co NPs (A) and $CoCl_2$ (B). C, Supplementation of cells with N-acetyl cysteine (NAC, 2.5 mM) rescued Co-mediated cell death at 12 hours. Co NPs and $CoCl_2$ reduced the protein and gene expression of ferroptosis regulators after 24 hours of exposure at 20 µg/mL: RT-PCR for *GPX4* (D), and *SLC7A11* (E), and quantification of western blot results for GPX4 protein (F) (refer to Suppl. Figure S4). Data shown are mean values ± SD (n = 3). *$P < .05$, **$P < .01$, **$P < .001$. Statistical significance determined by applying Tukey's *post hoc* multiple comparison test

NPs showed the most significant correlation with PD with a similarity index (SI) between NP and chemical (MPTP) of 0.99, while the SI between drug (L-dopa) and NP was 0.75.[12] The database did not contain data on Co NPs, only WC-Co NPs. Nevertheless, to further explore these associations, we retrieved the gene expression data from which these similarities had been computed. As shown in Figure S5B, *RAF1* (a proto-oncogene) and *NEFH* (neurofilament heavy) genes were found to be upregulated in the case of WC-Co NPs and MPTP and were downregulated in response to L-dopa. We then evaluated the expression of these genes in RA-differentiated SH-SY5Y cells, an accepted in vitro model of dopaminergic neurons.[19] To this end, cells were exposed to a sub-cytotoxic dose (5 µg/mL) of WC,

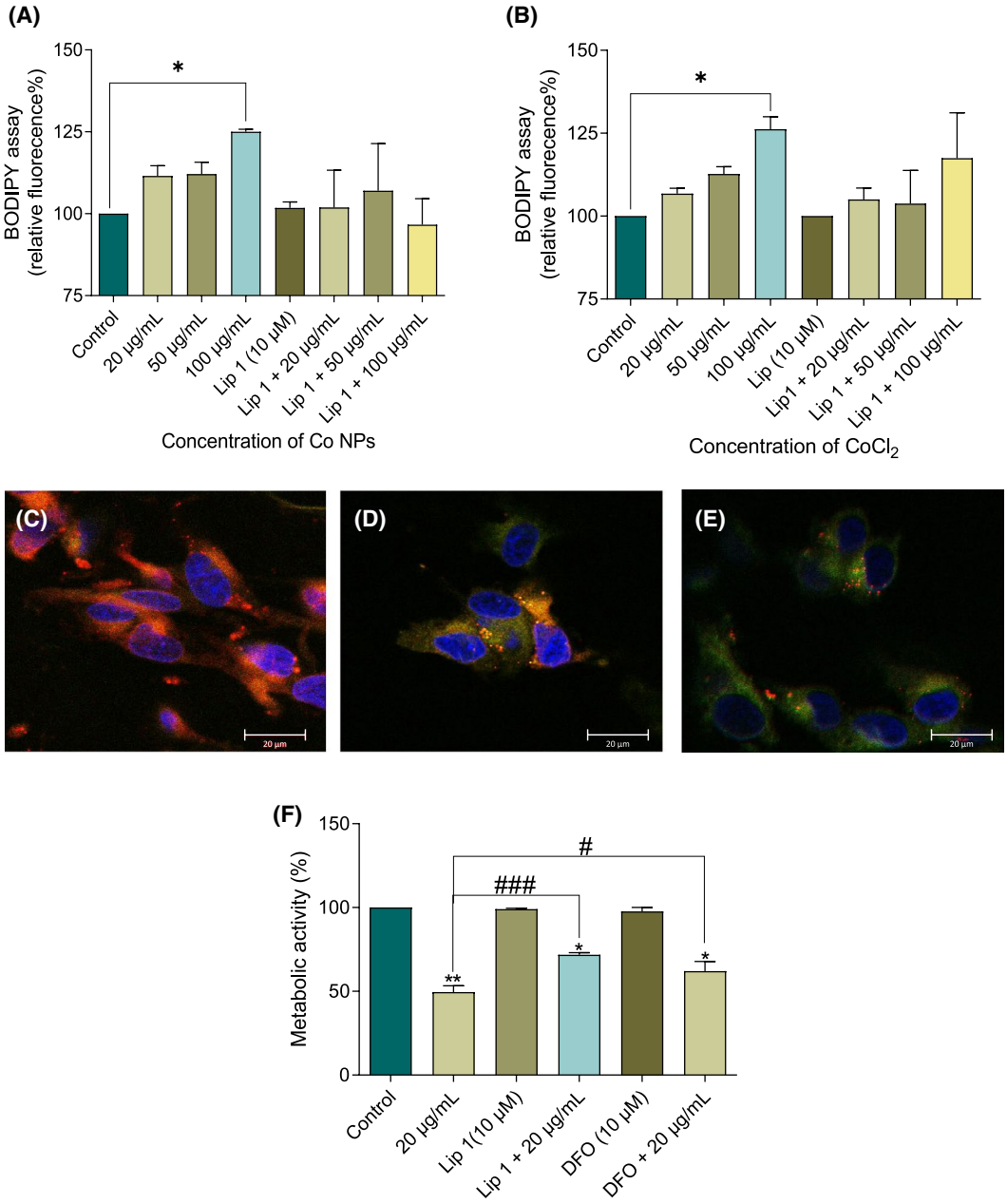

FIGURE 7 Co causes ferroptosis-like cell death (oxytosis) in undifferentiated SH-SY5Y cells. A-B, Lipid peroxidation in cells exposed to Co NPs and $CoCl_2$ at 20 µg/mL was determined by using the C11-BODIPY$_{581/591}$ assay. The relative C11-BODIPY$_{581/591}$ fluorescence was quantified in cells exposed to Co NPs (A) and $CoCl_2$ (B) in the presence and absence of Lip-1 (10 µM). Below are representative examples of cells stained with the C11-BODIPY$_{581/591}$ probe: C, control, D, Co NPs, E, $CoCl_2$. The shift from red to green fluorescence is reflective of the oxidation of the C11-BODIPY$_{581/591}$ probe. F, The lipid antioxidant, liproxstatin-1 (Lip-1, 10 µM), and the iron-chelating agent, deferoxamine (DFO, 10 µM), partially prevented Co NP-induced cell death. Data shown as mean values ± SD $^*P < .05$, $^{**}P < .01$, $^{**}P < .001$. Statistical significance between Lip-1 and DFO preexposed and unexposed groups determined by applying Tukey's multiple comparison test

WC-Co, and Co NPs *versus* $CoCl_2$ and the expression of *RAF1* and *NEFH* mRNA was determined by RT-PCR at day 6 of differentiation. WC-Co and Co NP as well as $CoCl_2$ exposed cells showed upregulation of both genes with respect to control, thereby validating the in silico predictions, while no changes in the expression of these genes were seen in WC NP-exposed cells (Figure S5C,D).

3.8 | Co induces cell death and axonal disintegration

To verify the findings obtained using the SH-SY5Y cell line, we performed experiments in primary dopaminergic neurons derived from a human iPSC line. The mature dopaminergic neurons at day 12 of differentiation contained >90%

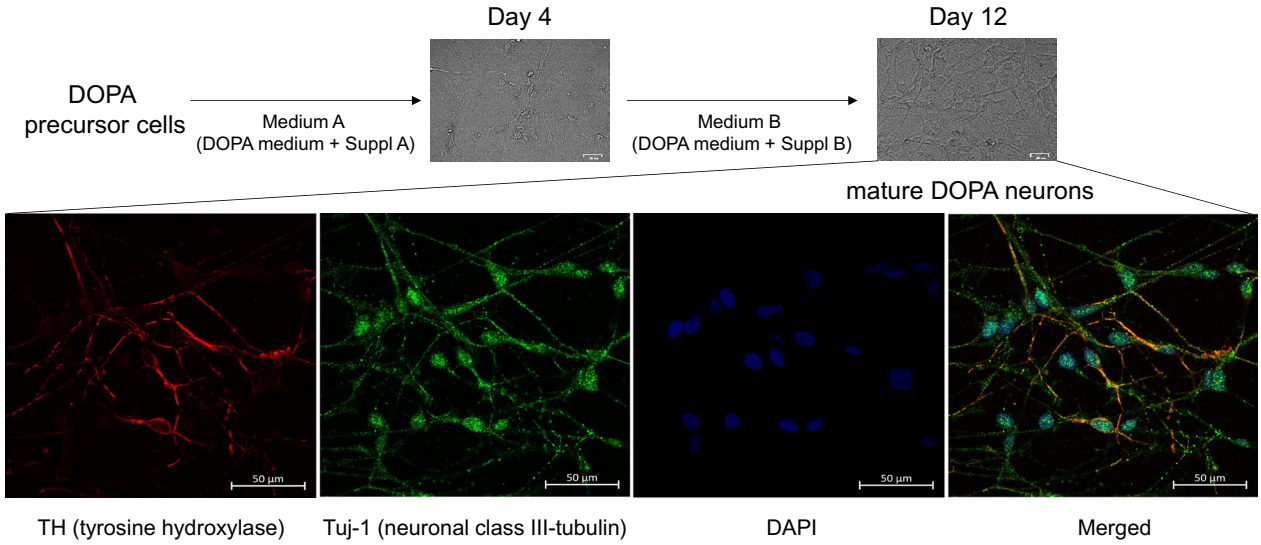

FIGURE 8 Primary dopaminergic precursors (day 4) and mature dopaminergic neurons (day 12) were derived from a human iPSC line. Mature DOPA neurons were positive for tyrosine hydroxylase (TH) and Tuj-1 (neuronal class III-tubulin). Cell nuclei visualized with DAPI

of Tuj-1 (neuronal class III β-tubulin) positive and >30% of TH-positive cells and displayed a well-developed axonal network (Figure 8). Importantly, a significant decrease in metabolic activity of 4-day dopaminergic precursors was observed following exposure to 20 µg/mL of Co NPs and its corresponding salt ($CoCl_2$) while no cytotoxicity was detected for WC and WC-Co NPs (Figure 9A). Furthermore, a decrease in GSH levels was detected in dopaminergic precursors exposed to Co NPs and the Co salt at 20 µg/mL (Figure 9B). Additionally, 12-day mature dopaminergic neurons also showed a significant decrease in cell viability after Co NPs and Co salt exposure, albeit less than that observed in 4-day DOPA precursors (Figure 9C). GSH depletion in mature dopaminergic neurons was, however, more pronounced than in the 4-day precursor neurons after Co NP and Co salt exposure (Figure 9D). It is worth noting that low-dose exposure (5 µg/mL) elicited an increased metabolic activity in mature DOPA neurons while no differences were seen in the DOPA precursors (Figure 9A,C). Optical micrographs of both 4-day and 12-day neurons showed dying/dead cells with altered axonal network after Co NP and $CoCl_2$ exposure (20 µg/mL). Untreated cells, on the contrary, were intact and displayed well-developed neurites and axonal network (Figure 9E). Finally, a higher dose of exposure (50 µg/mL) to Co NPs and $CoCl_2$ triggered a further increase in cytotoxicity of mature DOPA neurons, as determined by the Alamar blue assay, with complete disintegration of the axonal network and a rounding or blebbing of the cell soma (Figure S6A-D). We could not test the other NPs (WC and WC-Co) at this dose due to a limitation in the number of cells.

4 | DISCUSSION

We have shown herein that Co NPs and Co salt trigger dose-dependent cell death in neuronal cells through a non-apoptotic mechanism involving lipid peroxidation and depletion of GSH with downregulation of GPX4. Furthermore, when cells were exposed to a sub-cytotoxic dose of Co-containing NPs or Co salt, gene expression changes occurred that mirrored the changes observed in response to MPTP that yields PD-like symptoms in mice and humans. These results are relevant in light of previous case reports suggesting an association between Co poisoning and neurological disease.[24]

It is generally believed that Co^{2+} ions are able to produce hydroxyl radicals in the presence of hydrogen peroxide through a Fenton-like mechanism.[25] Furthermore, in the presence of WC particles, the reduction of oxygen in ROS by Co is catalyzed at the surface of WC particles leading to the release of large amounts of Co^{2+} ions.[26] Indeed, previous studies by Lison and coworkers have shown that WC-Co powder is more toxic toward murine macrophages in vitro than pure Co metal particles and that the cellular uptake of Co is enhanced when the metal is present in the form of WC-Co mixture.[27,28] Furthermore, the authors found that cellular Co uptake was higher when the metal was presented to macrophages as WC-Co as compared to Co alone. However, there was no relationship between the cellular uptake of Co and toxicity, indicating that increased bioavailability of Co is not the sole mechanism by which hard metal particles exhibit their cellular toxicity.[29] These studies were all conducted with professional phagocytic cells

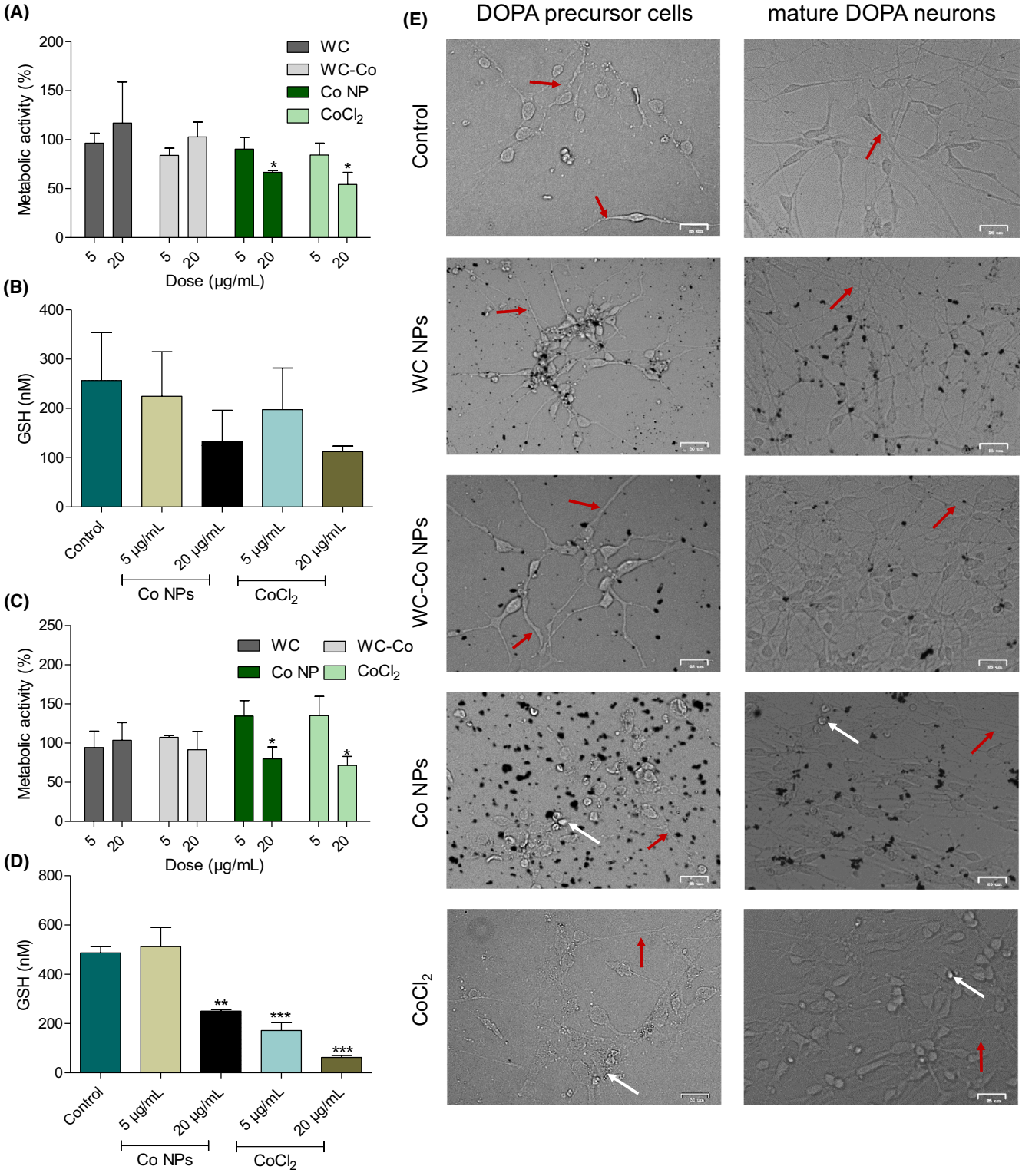

FIGURE 9 Co is cytotoxic for primary dopaminergic neurons. A, Metabolic activity, as determined by using the Alamar blue assay, and B, cellular GSH levels in differentiating DOPA precursor cells exposed for 24 hours to WC NPs, WC-Co NPs, Co NPs, and $CoCl_2$. C, Metabolic activity and D, cellular GSH level of mature DOPA neurons exposed for 24 hours to WC NPs, WC-Co NPs, Co NPs, and $CoCl_2$. E, Optical micrographs showing morphological features of DOPA precursors and mature DOPA neurons after exposure to 20 µg/mL of NPs or $CoCl_2$. Red arrows indicate axons and white arrows indicate dead or dying cells. Data in panel (A to D) are mean values ± SD (n = 3). $^{*}P < .05$, $^{**}P < .01$, $^{**}P < .001$. Statistical significance determined by applying Tukey's *post hoc* multiple comparison test

(macrophages). In contrast, in the present study, we found that NPs of Co elicited a drastic reduction in cell viability of neuronal cells while the impact of WC-Co NPs (5 wt% Co) was very modest and pure WC NPs were found to be non-cytotoxic. Moreover, ICP-MS analysis showed that the cellular content of Co was greater when cells were exposed to Co NPs as compared with the corresponding amount of $CoCl_2$ while Co NPs and $CoCl_2$ displayed a similar degree of toxicity in all three cell models (ie, undifferentiated, differentiating, and differentiated SH-SY5Y cells) thus underscoring that cellular content alone does not dictate the outcome. The bioavailability and/or subcellular compartmentalization of Co may certainly also come into play. TEM analysis suggested that Co NPs were enclosed in vesicles/endosomes while it is reasonable to assume that the metal ions are freely diffusible in the cell. The present study also suggests that cellular differentiation status may play a role as undifferentiated SH-SY5Y cells appeared to be more sensitive to Co NPs and $CoCl_2$ when compared to differentiated cells. Notably, a previous study has shown that the transcription factor Nrf2, a master regulator of the antioxidant response, is induced in SH-SY5Y cells upon RA-dependent neuronal differentiation.[30] Interestingly, a recent study has shown that silencing of Nrf2 aggravated the cell death induced in PC-12 cells by Co NPs and $CoCl_2$.[11]

Does oxidative stress play a role in Co-induced toxicity? Nyga et al[31] studied the toxicity of Co NPs using the macrophage-like U937 cell line, as well as human alveolar macrophages and monocyte-derived macrophages. They found that replenishing intracellular ascorbate reduced cytotoxicity and mitigated the inflammatory response while the addition of GSH had no effect on the Co-NP-induced cytotoxicity. On the contrary, Co NPs induced ROS formation in a concentration-dependent manner, and this was prevented by both ascorbic acid and GSH, suggesting that the ability of ascorbic acid to protect against Co NP-induced cytotoxicity was independent of its antioxidant activity.[31] In the present study, we found that Co NPs and $CoCl_2$-triggered ROS production and a dissipation of the mitochondrial membrane potential (at relatively high doses) yet ascorbic acid and mitoTEMPO did not afford any protection. Therefore, our current view is that while mitochondrial damage and ROS production may be considered as features of Co-induced cell death, these events are not the main instigators of cell death. Instead, a pronounced depletion of GSH levels was evidenced in cells exposed to Co NPs and $CoCl_2$, and the addition of NAC or GSH partially restored cell viability in exposed cells. Thus, oxidative stress, as indicated by the loss of GSH, plays an important role in the present model. Fenoglio et al[32] previously reported on the oxidation of GSH by hard metal dusts. This might lead to an irreversible depletion of antioxidant defenses, if this were to occur in cells. Co and WC alone, however, did not exhibit any reactivity toward GSH, and such a mechanism is unlikely to explain the depletion of GSH in the present model.

GSH levels are significantly depleted in the substantia nigra in PD.[33] Furthermore, using an in vitro model, Li et al[34] reported more than 20 years ago that a decrease in GSH triggers the activation of neuronal 12-lipoxygenase (12-LOX), which leads to the production of peroxides, influx of calcium, and subsequent cell death, suggesting a role for lipid peroxidation in neurodegeneration. Notably, in the present study, we have shown that Co NPs and Co salt elicit an influx of calcium in the neuronal SH-SY5Y cell line, and calcium chelators partially rescued the cells from Co-induced cell death. We also found that the lipid antioxidant, liproxstatin-1 reduced $CoCl_2$-mediated cell death and also afforded protection against Co NP-triggered cell death. Liproxstatin-1 was originally identified in a small molecule screen for ferroptosis inhibitors[35] and has been suggested to act as a radical trapping antioxidant[36]; it suppresses ferroptosis in *Gpx4*-deficient mice[35] and was recently shown to rescue the murine hippocampal cell line HT-22 from glutamate-triggered cell death.[37] In the present study, we provide evidence that Co-induced neurotoxicity transpires with a pronounced GSH depletion, along with calcium influx and lipid peroxidation. Moreover, we found that iron chelation suppressed Co-induced cell death, though the effects of deferoxamine and liproxstatin-1 were fairly modest. We can exclude apoptosis as the cells did not display any of the characteristic morphological features of apoptosis; moreover, the pan-caspase inhibitor, zVAD-fmk was not able to rescue the cells. Similarly, the necroptosis inhibitor, necrostatin-1 failed to block cell death. Instead, we observed mitochondrial swelling in cells exposed to Co NPs and the presence of fibrillary structures in the cytoplasm. Interestingly, glutamate-induced neurotoxicity is also accompanied by swollen mitochondria while the nuclei of glutamate-treated cells remain intact.[38] Taken together, our findings are indicative of a ferroptosis-like mode of cell death. Ferroptosis is defined as an iron-dependent form of regulated cell death that is linked to the accrual of lipid peroxides.[39] GPX4 has emerged as the main endogenous inhibitor of ferroptosis by virtue of its ability to limit lipid peroxidation; additionally, inhibition of the cystine/glutamate antiporter system x_c^- and the consequent decrease in GSH also triggers ferroptosis.[40] However, it is important to consider the fact that oxidative stress-induced death of neuronal cells with depletion of cellular GSH levels, referred to as oxytosis, was described in 2001, more than a decade before the first report on ferroptosis[41] and that the molecular pathways involved in the regulation of ferroptosis and oxytosis are very similar—if not identical.[42] Hence, both forms of cell death are regulated, non-apoptotic modes of cell death that are intimately linked to GSH depletion and calcium influx, and 12-LOX-mediated peroxidation appears to play a central role in the subsequent cell death.[42] It is pertinent to

note that we have shown here that Co-induced neurotoxicity is associated with a decrease in GPX4 expression both at the protein and mRNA level (indicating that Co exerts transcriptional effects in neuronal cells), thus implicating GPX4 in the regulation of oxytosis. Loss of GPX4 may compromise the cellular antioxidant defense leading to the accumulation of lethal lipid peroxides. Contrary to our expectations, we also observed an upregulation of the cystine/glutamate antiporter, system Xc^-, encoded by *SLC7A11*. In light of the depletion of GSH, we expected that the antiporter system would be downregulated. However, this could perhaps represent a compensatory mechanism resulting from the marked depletion of GSH in Co-exposed cells. The antiporter system Xc^- imports the amino acid cystine (the oxidized form of cysteine) into cells and exports glutamate. Cysteine, in turn, is the rate-limiting substrate in the synthesis of GSH.[43] Glutamate-induced neurotoxicity occurs when system Xc^- is inhibited[44] and it has been suggested that this cell death is a prototypic example of oxytosis.[43] Thus, Co elicits oxytosis, a ferroptosis-like mode of cell death, in neuronal cells, with features that resemble those of neuronal cells undergoing regulated cell death in neurodegenerative diseases. It is interesting to note that several genes that are involved in ferroptosis/oxytosis, including those encoding system Xc^- (*SLC7A11*) and GPX4, are transcriptionally regulated by Nrf2.[44] Nrf2 can also increase the expression of the multidrug resistance protein 1 (MRP1) that was shown recently to promote GSH efflux, thereby enhancing ferroptosis, which could counterbalance the protective effects of Nrf2-dependent GSH synthesis.[45] Further studies are required to pinpoint the role of Nrf2 in cell death, and whether transcriptional regulation by Nrf2 plays a role in ferroptosis/oxytosis in neurodegenerative disease.

It deserves to be mentioned that previous studies of oxytosis have shown that $CoCl_2$ protects against oxytosis at 20-50 μM and that this protection was suggested to be dependent on its ability to block calcium influx.[34,46,47] While in these studies, $CoCl_2$ alone did show some toxicity, it still provided significant protection against oxytosis. However, we believe that these apparent discrepancies are related to the dose of $CoCl_2$. Hence, 20-50 μM of $CoCl_2$[34,46] is likely too low to induce cytotoxicity, as toxicity was not observed in SH-SY5Y cells at 24 hours at 5 μg/mL (~20 μM) in the present study. In fact, in experiments using primary human dopaminergic neurons, we noted an increase in metabolic activity at 5 μg/mL, while cell viability was significantly decreased at doses of 20 and 50 μg/mL. Furthermore, it is important to consider not only the dose, but also the duration of exposure. Indeed, it is possible that long-term and/or repeated exposure at higher doses of Co NPs or $CoCl_2$ leads to ferroptosis/oxytosis, as shown in the present study.

Bastian et al[10] previously reported on the in vitro toxicity of WC and WC-Co (10 wt% Co) NPs and found that WC NPs did not yield any cytotoxicity up to 30 μg/mL after 3 days of exposure, while exposure to WC-Co NPs elicited slight toxicity for primary astrocytes derived from fetal rat cortices. Primary cortical neurons, on the contrary, were found to be resistant. Using iPSC-derived dopaminergic precursors and mature dopaminergic neurons, we show for the first time that Co NPs elicit significant cytotoxicity in primary human neurons along with a marked depletion of GSH levels. WC and WC-Co (5 wt% Co) were non-toxic in our model. Furthermore, we observed a loss of axonal integrity especially at high doses (50 μg/mL). Loss of the axonal network is considered a cardinal feature of the early stages of PD.[48,49] Other authors have presented evidence for a necroptosis-dependent pathway of axonal degeneration in an animal model of PD.[49] The present study does not refute this suggestion, though we can unequivocally conclude that cell death with loss of axonal integrity is linked to GSH depletion. It is interesting to note that the ablation of Gpx4 in forebrain neurons in mice was found to promote cognitive impairment and neuronal cell death with markers of ferroptosis (including lipid peroxidation),[50] further supporting the link between neurodegeneration and ferroptosis. Taken together, our results obtained in primary dopaminergic neurons serve to validate the results obtained using the SH-SY5Y model, and point toward a marked susceptibility of dopaminergic neurons and their precursors to Co.

To conclude, the present study demonstrated that Co NPs trigger dose-dependent cytotoxicity in a human neuronal cell line while WC NPs were non-cytotoxic and Co-doped WC NPs were only mildly cytotoxic. These findings were recapitulated in primary human dopaminergic neurons derived from iPS cells. Co salt ($CoCl_2$) was also markedly cytotoxic and the Co NPs were found to undergo rapid dissolution in cell culture; therefore, the toxicity of Co NPs in the present study is most likely associated with the release of Co^{2+} ions. Furthermore, our investigations have shown that the cell death displayed features of ferroptosis (referred to as oxytosis in earlier publications)[42] with depletion of the key cellular antioxidant, GSH as well as downregulation of GPX4. Furthermore, liproxstatin-1, a potent inhibitor of lipid peroxidation,[35] partially rescued the cells from Co-induced cell death, lending further support to a ferroptosis-like mechanism.

Could the present findings have any implications for human neurodegenerative diseases? Using the recently developed computational tool referred to as insideNANO,[12] we noted that Co-containing NPs were strongly linked to PD. The in silico-based predictions with respect to gene expression changes were validated in our in vitro model; however, the latter results are inferences based on similarities in gene expression profiles between different compounds, and do not constitute evidence per se of a link between Co poisoning and loss of dopaminergic neurons in the brain. On the contrary, the present observation that primary human dopaminergic neurons cultured

ex vivo are susceptible to Co NPs and Co salt with loss of axonal integrity shows that Co is, in fact, neurotoxic. Taken together, our results suggest that Co NPs may exert detrimental effects in neuronal cells, in particular in cells differentiated into dopaminergic neurons. Further studies are thus warranted to explore the potential link between Co-exposure and PD in humans. This is important in light of inadvertent occupational exposure to hard metals containing Co,[2] and biomedical applications including hip implants.[4]

ACKNOWLEDGMENTS

This work was supported by the Swedish Foundation for Strategic Environmental Research through the MISTRA Environmental Nanosafety program. The authors thank Dr Lars Haag, Electron Microscopy Core Facility, Karolinska Institutet, for TEM analyses of cells, and Dr Klara Midander, Karolinska Institutet, for assistance with the ICP-MS analysis.

CONFLICT OF INTEREST

The authors declare that they have no financial conflicts of interest in relation to this work.

AUTHOR CONTRIBUTIONS

G. Gupta performed all the in vitro experiments, analyzed data, and drafted the manuscript; A. Gliga and J. Hedberg performed particle characterization; A. Serra performed the in silico transcriptomics analysis under the supervision of D. Greco, I. O. Wallinder supervised the particle characterization; B. Fadeel conceived and coordinated the study and supervised the experimental work, and wrote the manuscript; all co-authors approved the final version of the paper.

REFERENCES

1. Lison D. Human toxicity of cobalt-containing dust and experimental studies on the mechanism of interstitial lung disease (hard metal disease). *Crit Rev Toxicol*. 1996;26(6):585-616.
2. Paustenbach DJ, Tvermoes BE, Unice KM, Finley BL, Kerger BD. A review of the health hazards posed by cobalt. *Crit Rev Toxicol*. 2013;43(4):316-362.
3. Furberg A, Arvidsson R, Molander S. Live and let die? Life cycle human health impacts from the use of tire studs. *Int J Environ Res Public Health*. 2018;15(8):1774.
4. Leyssens L, Vinck B, Van Der Straeten C, Wuyts F, Maes L. Cobalt toxicity in humans—a review of the potential sources and systemic health effects. *Toxicology*. 2017;387:43-56.
5. Keegan GM, Learmonth ID, Case CP. A systematic comparison of the actual, potential, and theoretical health effects of cobalt and chromium exposures from industry and surgical implants. *Crit Rev Toxicol*. 2008;38(8):645-674.
6. Estey MP, Diamandis EP, Van Der Straeten C, Tower SS, Hart AJ, Moyer TP. Cobalt and chromium measurement in patients with metal hip prostheses. *Clin Chem*. 2013;59(6):880-886.
7. Scharf B, Clement CC, Zolla V, et al. Molecular analysis of chromium and cobalt-related toxicity. *Sci Rep*. 2014;4:5729.
8. Rizzetti MC, Liberini P, Zarattini G, et al. Loss of sight and sound. Could it be the hip? *Lancet*. 2009;373:1052.
9. Woelber E, Van Citters DW, Steck T, Glass GA, Tower S. Explant analysis from a patient exhibiting rapid acceleration of Parkinson disease symptoms and hypercobaltemia following metal-on-metal total hip arthroplasty: a case report. *JBJS Case Connect*. 2016;6(2):e45.
10. Bastian S, Busch W, Kühnel D, et al. Toxicity of tungsten carbide and cobalt-doped tungsten carbide nanoparticles in mammalian cells *in vitro*. *Environ Health Perspect*. 2009;117(4):530-536.
11. Zheng F, Luo Z, Zheng C, et al. Comparison of the neurotoxicity associated with cobalt nanoparticles and cobalt chloride in Wistar rats. *Toxicol Appl Pharmacol*. 2019;369:90-99.
12. Serra A, Letunic I, Fortino V, et al. INSIdE NANO: a systems biology framework to contextualize the mechanism-of-action of engineered nanomaterials. *Sci Rep*. 2019;9(1):179.
13. Bhattacharya K, Kiliç G, Costa PM, Fadeel B. Cytotoxicity screening and cytokine profiling of nineteen nanomaterials enables hazard ranking and grouping based on inflammogenic potential. *Nanotoxicology*. 2017;11(6):809-826.
14. Hedberg YS, Hedberg JF, Isaksson S, et al. Nanoparticles of WC-Co, WC, Co and Cu of relevance for traffic wear particles—particle stability and reactivity in synthetic surface water and influence of humic matter. *Environ Pollut*. 2017;224:275-288.
15. Di Bucchianico S, Gliga AR, Åkerlund E, et al. Calcium-dependent cyto- and genotoxicity of nickel metal and nickel oxide nanoparticles in human lung cells. *Part Fibre Toxicol*. 2018;15(1):32.
16. Gallud A, Klöditz K, Ytterberg J, et al. Cationic gold nanoparticles elicit mitochondrial dysfunction: a multi-omics study. *Sci Rep*. 2019;9(1):4366.
17. Klöditz K, Fadeel B. Three cell deaths and a funeral: macrophage clearance of cells undergoing distinct modes of cell death. *Cell Death Discov*. 2019;8(5):65.
18. Kong L, Tuomela S, Hahne L, et al. NanoMiner—integrative human transcriptomics data resource for nanoparticle research. *PLoS ONE*. 2013;8(7):e68414.https://doi.org/10.1371/journal.pone.0068414
19. Korecka JA, van Kesteren RE, Blaas E, et al. Phenotypic characterization of retinoic acid differentiated SH-SY5Y cells by transcriptional profiling. *PLoS ONE*. 2013;8(5):e63862.
20. Roy S, Wolman L. Ultrastructural observations in Parkinsonism. *J Pathol*. 1969;99(1):39-44.
21. Llobet JM, Domingo JL, Corbella J. Comparison of the effectiveness of several chelators after single administration on the toxicity, excretion and distribution of cobalt. *Arch Toxicol*. 1986;58(4):278-281.
22. Murphy TH, Miyamoto M, Sastre A, Schnaar RL, Coyle JT. Glutamate toxicity in a neuronal cell line involves inhibition of cystine transport leading to oxidative stress. *Neuron*. 1989;2(6):1547-1555.
23. Seiler A, Schneider M, Förster H, et al. Glutathione peroxidase 4 senses and translates oxidative stress into 12/15-lipoxygenase dependent- and AIF-mediated cell death. *Cell Metab*. 2008;8(3):237-248.
24. Catalani S, Rizzetti MC, Padovani A, Apostoli P. Neurotoxicity of cobalt. *Hum Exp Toxicol*. 2012;31(5):421-437.

25. Lison D.Cobalt. In: Nordberg GF, Fowler BA, Nordberg M. *Handbook on the Toxicology of Metals*. 4th ed. Academic Press-Elsevier; 2015:743-763.
26. Lison D, Carbonnelle P, Mollo L, Lauwerys R, Fubini B. Physicochemical mechanism of the interaction between cobalt metal and carbide particles to generate toxic activated oxygen species. *Chem Res Toxicol*. 1995;8(4):600-606.
27. Lison D, Lauwerys R *In vitro* cytotoxic effects of cobalt-containing dusts on mouse peritoneal and rat alveolar macrophages. *Environ Res*. 1990;52(2):187-198.
28. Lison D, Lauwerys R. Study of the mechanism responsible for the elective toxicity of tungsten carbide-cobalt powder toward macrophages. *Toxicol Lett*. 1992;60(2):203-210.
29. Lison D, Lauwerys R. Cobalt bioavailability from hard metal particles. Further evidence that cobalt alone is not responsible for the toxicity of hard metal particles. *Arch Toxicol*. 1994;68(8):528-531.
30. Zhao F, Wu T, Lau A, et al. Nrf2 promotes neuronal cell differentiation. *Free Radic Biol Med*. 2009;47(6):867-879.
31. Nyga A, Hart A, Tetley TD. Importance of the HIF pathway in cobalt nanoparticle-induced cytotoxicity and inflammation in human macrophages. *Nanotoxicology*. 2015;9(7):905-917.
32. Fenoglio I, Corazzari I, Francia C, Bodoardo S, Fubini B. The oxidation of glutathione by cobalt/tungsten carbide contributes to hard metal-induced oxidative stress. *Free Radic Res*. 2008;42(8):437-745.
33. Sian J, Dexter DT, Lees AJ, et al. Alterations in glutathione levels in Parkinson's disease and other neurodegenerative disorders affecting basal ganglia. *Ann Neurol*. 1994;36(3):348-355.
34. Li Y, Maher P, Schubert D. A role for 12-lipoxygenase in nerve cell death caused by glutathione depletion. *Neuron*. 1997;19(2):453-463.
35. Friedmann Angeli JP, Schneider M, Proneth B, et al. Inactivation of the ferroptosis regulator Gpx4 triggers acute renal failure in mice. *Nat Cell Biol*. 2014;16(12):1180-1191.
36. Zilka O, Shah R, Li B, et al. On the mechanism of cytoprotection by ferrostatin-1 and liproxstatin-1 and the role of lipid peroxidation in ferroptotic cell death. *ACS Cent Sci*. 2017;3(3):232-243.
37. Neitemeier S, Jelinek A, Laino V, et al. BID links ferroptosis to mitochondrial cell death pathways. *Redox Biol*. 2017;12:558-570.
38. Tan S, Wood M, Maher P. Oxidative stress induces a form of programmed cell death with characteristics of both apoptosis and necrosis in neuronal cells. *J Neurochem*. 1998;71(1):95-105.
39. Dixon SJ, Lemberg KM, Lamprecht MR, et al. Ferroptosis: an iron-dependent form of nonapoptotic cell death. *Cell*. 2012;149(5):1060-1072.
40. Stockwell BR, Friedmann Angeli JP, Bayir H, et al. Ferroptosis: a regulated cell death nexus linking metabolism, redox biology, and disease. *Cell*. 2017;171(2):273-285.
41. Tan S, Schubert D, Maher P. Oxytosis: a novel form of programmed cell death. *Curr Top Med Chem*. 2001;1(6):497-506.
42. Lewerenz J, Ates G, Methner A, Conrad M, Maher P. Oxytosis/ferroptosis-(re-) emerging roles for oxidative stress-dependent non-apoptotic cell death in diseases of the central nervous system. *Front Neurosci*. 2018;12:214.
43. Lewerenz J, Hewett SJ, Huang Y, et al. The cystine/glutamate antiporter system x_c^- in health and disease: from molecular mechanisms to novel therapeutic opportunities. *Antioxid Redox Signal*. 2013;18(5):522-555.
44. Abdalkader M, Lampinen R, Kanninen KM, Malm TM, Liddell JR. Targeting Nrf2 to suppress ferroptosis and mitochondrial dysfunction in neurodegeneration. *Front Neurosci*. 2018;12:466.
45. Cao JY, Poddar A, Magtanong L, et al. A genome-wide haploid genetic screen identifies regulators of glutathione abundance and ferroptosis sensitivity. *Cell Rep*. 2019;26(6):1544-1556.e8.
46. Tan S, Sagara Y, Liu Y, Maher P, Schubert D. The regulation of reactive oxygen species production during programmed cell death. *J Cell Biol*. 1998;141(6):1423-1432.
47. Davis JB, Maher P. Protein kinase C activation inhibits glutamate-induced cytotoxicity in a neuronal cell line. *Brain Res*. 1994;652(1):169-173.
48. Li Y, Liu W, Oo TF, et al. Mutant *LRRK2*^{R1441G} BAC transgenic mice recapitulate cardinal features of Parkinson's disease. *Nat Neurosci*. 2009;12(7):826-828.
49. Oñate M, Catenaccio A, Salvadores N, et al. The necroptosis machinery mediates axonal degeneration in a model of Parkinson disease. *Cell Death Differ*. 2019. https://doi.org/10.1038/s41418-019-0408-4. [Epub ahead of print].
50. Hambright WS, Fonseca RS, Chen L, Na R, Ran Q. Ablation of ferroptosis regulator glutathione peroxidase 4 in forebrain neurons promotes cognitive impairment and neurodegeneration. *Redox Biol*. 2017;12:8-17.

SUPPORTING INFORMATION

Additional Supporting Information may be found online in the Supporting Information section.

How to cite this article: Gupta G, Gliga A, Hedberg J, et al. Cobalt nanoparticles trigger ferroptosis-like cell death (oxytosis) in neuronal cells: Potential implications for neurodegenerative disease. *The FASEB Journal*. 2020;00:1–20. https://doi.org/10.1096/fj.201902191RR